



Carbon–Concentration and Carbon–Climate Feedbacks in CMIP5 Earth System Models

VIVEK K. ARORA,^a GEORGE J. BOER,^a PIERRE FRIEDLINGSTEIN,^b MICHAEL EBY,^c CHRIS D. JONES,^d JAMES R. CHRISTIAN,^a GORDON BONAN,^c LAURENT BOPP,^f VICTOR BROVKIN,^g PATRICIA CADULE,^f TOMOHIRO HAJIMA,^h TATIANA ILYINA,^g KEITH LINDSAY,^c JERRY F. TJIPUTRA,ⁱ AND TONGWEN WU^j

^a Canadian Centre for Climate Modelling and Analysis, Environment Canada, University of Victoria, Victoria, British Columbia, Canada

^b College of Engineering, Mathematics and Physical Sciences, University of Exeter, Exeter, United Kingdom

^c School of Earth and Ocean Sciences, University of Victoria, Victoria, British Columbia, Canada

^d Met Office Hadley Centre, Exeter, United Kingdom

^e National Center for Atmospheric Research,^k Boulder, Colorado

^f LSCE, IPSL, CEA, UVSQ, CNRS, Gif-sur-Yvette, France

^g Max Planck Institute for Meteorology, Hamburg, Germany

^h Research Institute for Global Change, Japan Agency for Marine–Earth Science and Technology, Yokohama, Japan

ⁱ Uni Klima, Uni Research, Bergen, Norway

^j Beijing Climate Center, China Meteorological Administration, Beijing, China

(Manuscript received 24 July 2012, in final form 5 February 2013)

ABSTRACT

The magnitude and evolution of parameters that characterize feedbacks in the coupled carbon–climate system are compared across nine Earth system models (ESMs). The analysis is based on results from biogeochemically, radiatively, and fully coupled simulations in which CO₂ increases at a rate of 1% yr^{−1}. These simulations are part of phase 5 of the Coupled Model Intercomparison Project (CMIP5). The CO₂ fluxes between the atmosphere and underlying land and ocean respond to changes in atmospheric CO₂ concentration and to changes in temperature and other climate variables. The carbon–concentration and carbon–climate feedback parameters characterize the response of the CO₂ flux between the atmosphere and the underlying surface to these changes. Feedback parameters are calculated using two different approaches. The two approaches are equivalent and either may be used to calculate the contribution of the feedback terms to diagnosed cumulative emissions. The contribution of carbon–concentration feedback to diagnosed cumulative emissions that are consistent with the 1% increasing CO₂ concentration scenario is about 4.5 times larger than the carbon–climate feedback. Differences in the modeled responses of the carbon budget to changes in CO₂ and temperature are seen to be 3–4 times larger for the land components compared to the ocean components of participating models. The feedback parameters depend on the state of the system as well as the forcing scenario but nevertheless provide insight into the behavior of the coupled carbon–climate system and a useful common framework for comparing models.

1. Introduction

Earth system models (ESMs) incorporate terrestrial and ocean carbon cycle processes into coupled

atmosphere–ocean general circulation models (AOGCMs) in order to represent the interactions between the carbon cycle and the physical climate system. Changes in the physical climate affect the exchange of CO₂ between the atmosphere and the underlying land and ocean, and the resulting changes in atmospheric concentration of CO₂ in turn affect the physical climate. Aspects of the behavior of the carbon cycle and its interaction with the physical climate system are characterized in terms of carbon–concentration and carbon–climate feedback parameters (Friedlingstein et al. 2006; Boer and Arora 2009; Roy et al. 2011). Feedback parameters can be calculated

^k The National Center for Atmospheric Research is sponsored by the National Science Foundation.

Corresponding author address: Vivek K. Arora, Canadian Centre for Climate Modelling and Analysis, Environment Canada, University of Victoria, Victoria BC V8W 2Y2, Canada.
E-mail: vivek.arora@ec.gc.ca

for global averages, separately over land and ocean, over specific regions or for individual grid cells in order to investigate their geographical distribution as in Boer and Arora (2010). The carbon–concentration feedback parameter is a measure of the response of the land and ocean carbon pools to changes in atmospheric CO₂ concentration. It is a negative feedback from the perspective of the atmosphere, since the higher values of atmospheric CO₂ that result from anthropogenic emissions are partially offset by a loss of atmospheric carbon to the underlying land and ocean. The carbon–climate feedback parameter is a measure of the response to changes in temperature and other climate variables. The carbon–climate feedback parameter is generally positive from the atmosphere’s perspective as higher temperatures promote a flux of carbon from the land and ocean into the atmosphere. The positive carbon–climate feedback acts to reduce the capacity of the land and ocean to take up carbon resulting in a larger fraction of anthropogenic CO₂ emissions remaining in the atmosphere as temperatures warm. The first Coupled Carbon Cycle Climate Model Intercomparison Project (C⁴MIP) found that this positive carbon–climate feedback varied significantly across ESMs due mainly to the differences in the behavior of terrestrial carbon cycle components (Friedlingstein et al. 2006).

Both carbon–climate and, in particular, carbon–concentration feedback parameters have been found to be sensitive to the emission scenario, the state of the system, and the approach used to calculate them (Boer and Arora 2009, 2010; Plattner et al. 2008; Gregory et al. 2009; Zickfeld et al. 2011). As a result, values of feedback parameters from one scenario cannot be used, in a quantitative way, to project carbon cycle behavior for a different emission scenario. The geographical patterns of the feedback parameters are, however, found to be reasonably robust across different emissions scenarios (Boer and Arora 2010) and the feedback parameters do serve to illustrate and quantify the carbon feedback processes operating in the coupled carbon–climate system. The dependence of the feedback parameters on emission scenario and system state means that the comparison of the behavior of the coupled carbon–climate system across models is more straightforwardly investigated for a common scenario.

The fifth phase of the Coupled Model Intercomparison Project (CMIP5; <http://cmip-pcmdi.llnl.gov/cmip5/forcing.html>) (Taylor et al. 2012) provides a common framework for comparing and assessing Earth system processes in the context of climate simulations. A 140-yr-long simulation in which atmospheric CO₂ concentration increases at a rate of 1% yr^{−1} from preindustrial values until concentration quadruples is a standard

CMIP experiment that serves to quantify the response to increasing CO₂. To isolate feedbacks, additional radiatively and biogeochemically coupled versions of this “1% increasing CO₂” experiment are performed. In radiatively coupled simulations increasing atmospheric CO₂ affects the climate but not the biogeochemistry, for which the preindustrial value of atmospheric CO₂ concentration is prescribed. In the biogeochemically coupled simulation the biogeochemistry responds to the increasing atmospheric CO₂ while the radiative forcing remains at preindustrial values. The simulations do not include the confounding effects of changes in land use, non-CO₂ greenhouse gases, aerosols, etc., and so provide a controlled experiment with which to compare carbon–climate interactions across models. Results from eight of the comprehensive Earth system models participating in the CMIP5 intercomparison project are analyzed as well as results from an Earth system model of intermediate complexity (EMIC).

2. Feedbacks in the coupled climate–carbon system

We consider globally averaged and vertically integrated carbon budget quantities. Following Boer and Arora (2013) for the combined atmosphere–land–ocean system the rate of change of carbon is written as

$$\frac{dH_G}{dt} = \frac{dH_A}{dt} + \frac{dH_L}{dt} + \frac{dH_O}{dt} = E, \quad (1)$$

where the global carbon pool $H_G = H_A + H_L + H_O$ is the sum of carbon in the atmosphere, land, and ocean components (Pg C) and E is the rate of anthropogenic CO₂ emission (Pg C yr^{−1}) into the atmosphere. The equations for the atmosphere, land, and ocean are

$$\begin{aligned} \frac{dH_A}{dt} &= F_A(T, C) + E, \\ \frac{dH_L}{dt} &= F_L(T, C), \quad \text{and} \\ \frac{dH_O}{dt} &= F_O(T, C), \end{aligned} \quad (2)$$

where $(F_L + F_O) = -F_A$ are the fluxes between the atmosphere and the underlying land and ocean, taken to be positive into the components. The fluxes F are expressed as functions of surface temperature T and the surface atmospheric CO₂ concentration C , following Boer and Arora (2009, 2010). In the experiments analyzed here the CO₂ concentration is specified beginning at the preindustrial value of ~285 ppm and increasing at

1% yr⁻¹ until concentration has quadrupled 140 years later. The rate of change of atmospheric carbon dH_A/dt is specified in (1) and (2) and the loss or gain of CO₂ by the underlying land and ocean yields an effective emission E , which serves to maintain the budget.

a. Direct/instantaneous feedback parameters

Following Boer and Arora (2009, 2010) and the accompanying paper by Boer and Arora (2013, hereafter BA), the changes in atmosphere carbon budgets, from the control simulation, in the differently coupled simulations are represented as follows:

- radiatively coupled

$$\frac{dH'_A}{dt} - E^+ = F'_A = \Gamma_A T^+, \quad (3a)$$

- biogeochemically coupled

$$\frac{dH'_A}{dt} - E^* = F'_A = \Gamma_A T^* + B_A C', \quad \text{and} \quad (3b)$$

- fully coupled

$$\frac{dH'_A}{dt} - E = F'_A = -F'_L - F'_O = \Gamma_A T' + B_A C', \quad (3c)$$

which serve to define the carbon–concentration (B_A) and carbon–climate (Γ_A) feedback parameters and assume an approximately linear response of the globally integrated surface–atmosphere CO₂ flux in terms of global mean temperature and CO₂ concentration change. The control simulation has no anthropogenic emissions and a specified atmospheric CO₂ concentration C_0 of ~285 ppm. In Eq. (3), F^+ , F^* , and F' are the flux changes; T^+ , T^* , and T' are the temperature changes in the radiatively, biogeochemically, and fully coupled simulations; and E^+ , E^* , and E are the resulting implicit emissions. In the biogeochemically coupled simulation there is no radiative forcing because of increasing CO₂ so T^* is small, although it is not zero. Changes in vegetation biomass and transpiration as well as vegetation structure (e.g., changes in leaf area index and vegetation height) and its spatial distribution (through competition between plant functional types) affect the surface energy and water balance to some extent. Changes in absorption of solar radiation can also affect climate through changes in phytoplankton and chlorophyll although phytoplankton growth parameterizations usually do not include a strong dependence on CO₂. The term $H'_A = mC'$ is the change in atmosphere CO₂ amount (Pg C), which is the same for the biogeochemically, radiatively, and fully coupled versions since C' is specified.

The term m is the mass of the atmosphere multiplied by the ratio of molecular weight of carbon to the mean molecular weight of air.¹ Although the feedback parameters are dependent on the approach used to calculate them and also if they are determined from emissions- or concentration-driven simulations (Gregory et al. 2009; Zickfeld et al. 2011; Boer and Arora 2013), the assumption made in Eq. (3) is that the feedback parameters are the same in the three cases. It is a reasonable assumption for the 1% CO₂ simulations considered here, as is shown later.

Carbon budget changes for the land component parallel (3) but without the emissions terms as

- radiatively coupled

$$\frac{dH'_L}{dt} = F'_L = \Gamma_L T^+, \quad (4a)$$

- biogeochemically coupled

$$\frac{dH'_L}{dt} = F'_L = \Gamma_L T^* + B_L C', \quad \text{and} \quad (4b)$$

- fully coupled

$$\frac{dH'_L}{dt} = F'_L = \Gamma_L T' + B_L C', \quad (4c)$$

and similarly for the ocean component. Since $F_A = -(F_L + F_O)$, it follows that $\Gamma_A = -(\Gamma_L + \Gamma_O)$ and $B_A = -(B_L + B_O)$.

The feedback parameters Γ and B represent averaged rates of change of the CO₂ flux F with respect to temperature and concentration and indicate how the system responds to temperature and CO₂ concentration changes [see section 3d in Boer and Arora (2013)]. There are no terms involving C' in the radiatively coupled simulation [Eqs. (3a) and (4a)] since the pre-industrial value of atmospheric CO₂ concentration is prescribed for the biogeochemistry components so $C' = 0$ and does not affect the flux. Changes in the flux in the radiatively coupled simulation are driven by changes in temperature alone.

b. Integrated flux-based feedback parameters

The flux-based BA approach in section 2a differs from the integrated flux approach of Friedlingstein

¹ $m = 5.1 \times 10^{18} \times (12.01/28.93) \approx 2.12 \times 10^{18} \text{ kg} = 2.12 \times 10^6 \text{ Pg}$, where $5.1 \times 10^{18} \text{ kg}$ is the mass of the atmosphere: 12.01 and 28.93 are the molecular weights (g mol⁻¹) of carbon and air, respectively, and 1 ppmv CO₂ (1×10^{-6} volume mixing ratio) in the atmosphere is thus equivalent to $2.12 \times 10^{12} \text{ kg C}$ (or 2.12 Pg C).

et al. (2006), who express time-integrated flux changes (i.e., change in pool or reservoir sizes) as functions of temperature and CO₂ concentration changes (referred to as the FEA approach) with

- radiatively coupled

$$\int F_A^+ dt = \gamma_A T^+, \quad (5a)$$

- biogeochemically coupled

$$\int F_A^* dt = \gamma_A T^* + \beta_A C', \quad \text{and} \quad (5b)$$

- fully coupled

$$\int F_A' dt = \gamma_A T' + \beta_A C' \quad (5c)$$

and similarly for the land and ocean components. The connection between γ and β in (5) and Γ and B in (3) is

$$\gamma_A = \frac{\int_0^t \Gamma_A T^+ dt}{T^+} \quad (6a)$$

from the radiatively coupled cases (3a) and (5a); for small T^* the biogeochemically coupled simulations (3b) and (5b) give

$$\beta_A = \frac{\int_0^t (\Gamma_A T^* + B_A C') dt - \gamma_A T^*}{C'} \approx \frac{\int_0^t B_A C' dt}{C'}. \quad (6b)$$

The FEA parameters are temperature (T^+) and CO₂ concentration change (C') weighted versions of the BA feedback parameters. As shown in appendix A, Eqs. (3) and (5) with two unknowns each are consistent provided that the system is linear (i.e., $F' = F^+ + F^*$ and $T' = T^+ + T^*$), so that the fully coupled case is the sum of the radiatively and biogeochemically coupled cases for seven of the nine models considered. For the comparison of feedback parameters among models, we use results from the radiatively and biogeochemically coupled simulations that have only one component, either radiation or biogeochemistry, responding to increasing CO₂ and that are designed to isolate the two feedbacks.

c. Feedback contributions

Integrating Eqs. (1) and (2) from initial time to t gives

$$H'_A + H'_L + H'_O = \int_0^t E dt = \tilde{E}, \quad (7)$$

where $H'_A = H'_A(t) - H'_A(0)$ is the change in atmospheric carbon burden and $H'_X = \int_0^t F'_X dt$, where $X = L, O$ is the cumulative flux equal to the change in the land or ocean carbon pool for the fully coupled simulation. The terms in Eq. (7) indicate the contribution of cumulative emissions \tilde{E} to the atmosphere, land, and ocean carbon pools.

As discussed in the accompanying manuscript by Boer and Arora (2013), the different units for the feedback parameters Γ (Pg C yr⁻¹ °C⁻¹), B (Pg C yr⁻¹ ppm⁻¹), γ (Pg C °C⁻¹), and β (Pg C ppm⁻¹) mean that their respective contributions to the atmospheric carbon budget are not immediately obvious. Following Eq. (3) and the assumed linearization of the globally integrated surface-atmosphere CO₂ flux in terms of global mean temperature and CO₂ concentration, these contributions may be estimated by decomposing the flux changes into components associated with the carbon-concentration (F_C) and carbon-climate (F_T) feedbacks using $F'_A = F_C + F_T = B_A C' + \Gamma_A T'$ and writing

$$H'_A + H'_C + H'_T = \tilde{E}_e = \tilde{E} + \delta\tilde{E}, \quad (8)$$

where $H'_C = -\int_0^t B_A C' dt = \int_0^t (B_L + B_O) C' dt = -\beta_A C' = (\beta_L + \beta_O) C'$ and $H'_T = -\int_0^t \Gamma_A T' dt = \int_0^t (\Gamma_L + \Gamma_O) T' dt = -\gamma_A T' = (\gamma_L + \gamma_O) T'$ are the cumulative flux changes associated with the carbon-concentration and carbon-climate feedbacks, respectively. The term $\delta\tilde{E}$ is the difference between $\int_0^t F'_A dt$ and its approximation as $H'_C + H'_T = -\int_0^t (B_A C' + \Gamma_A T') dt = -(\beta_A C' + \gamma_A T')$. With $B_A = -(B_L + B_O)$ and $\Gamma_A = -(\Gamma_L + \Gamma_O)$, Eq. (8) can be further decomposed to obtain land and ocean components of the feedbacks as

$$H'_A + H'_{TL} + H'_{CL} + H'_{TO} + H'_{CO} = \tilde{E}_e = \tilde{E} + \delta\tilde{E}, \quad (9)$$

where $H'_{TL} = \int_0^t \Gamma_L T' dt = \gamma_L T'$ and $H'_{CL} = \int_0^t B_L C' dt = \beta_L C'$ and similarly for the ocean terms. Finally, division by the respective cumulative emissions term in Eqs. (7)–(9) gives all the terms in a fractional form as

$$f_A + f_L + f_O = 1 \quad \text{and} \quad (10)$$

$$f_A + f_C + f_T = f_A + f_{CL} + f_{CO} + f_{TL} + f_{TO} = 1, \quad (11)$$

where f_A is the airborne fraction of cumulative emissions and f_L and f_O are the fractions of emissions taken up by the land and ocean, respectively. The terms f_C and f_T are the fractional contributions to diagnosed cumulative emissions associated with carbon-concentration and carbon-climate feedbacks and f_{CL} , f_{TL} , f_{CO} , and f_{TO} are their land and ocean components. These components can be calculated using either the BA or the FEA approach and are evaluated at the time of CO₂ quadrupling.

d. Gain

Friedlingstein et al. (2003, 2006) quantify the effect of carbon–climate feedback in their emission-driven simulations in terms of gain (g) as

$$\frac{C'}{C^*} = \frac{1}{1-g}, \quad g = \frac{C' - C^*}{C'}, \quad (12)$$

where C' and C^* are the simulated atmospheric CO_2 concentrations for the fully and biogeochemically coupled cases. A positive g implies that $C' > C^*$. The simulations analyzed here specify concentrations so $C' = C^*$ and (12) cannot be used as a measure of gain. An analogous quantity g_E may be defined using cumulative implied emissions from the fully (\tilde{E}) and biogeochemically coupled (\tilde{E}^*) simulations as

$$g_E = \frac{\tilde{E}^* - \tilde{E}}{\tilde{E}^*}. \quad (13)$$

This is broadly consistent with the discussion in the accompanying Boer and Arora (2013, their section 3), who note the roles of dH_A/dt versus E terms in the emission- and concentration-driven cases. A positive g_E implies that $\tilde{E}^* > \tilde{E}$: that is, implied emissions in the biogeochemically coupled simulation are higher than the fully coupled case because the carbon–climate feedback is absent in the biogeochemically coupled simulation.

Integrating Eq. (3b) for the biogeochemically coupled case and assuming T^* is zero (since temperature change T^* in the biogeochemically coupled case is small) gives an estimate of \tilde{E}^* similar to Eq. (8),

$$H'_A + H'_C = \tilde{E}^* = \tilde{E} + \delta\tilde{E}^*, \quad (14)$$

where $\delta\tilde{E}^*$ reflects the difference between $\int_0^t F_A^* dt$ and its approximation as $H'_C = -\int_0^t B_A C' dt = -\beta_A C'$ and the assumption that $T^* = 0$. Solving Eqs. (8), (13), and (14) and assuming $\delta\tilde{E} \approx 0$, $\delta\tilde{E}^* \approx 0$ gives an estimate of g_E in terms of both BA and FEA feedback parameters as

$$\begin{aligned} \hat{g}_E &= \frac{\int_0^t \Gamma_A T' dt}{mC' - \int_0^t B_A C' dt} = \frac{\gamma_A T'}{C'(m - \beta_A)} \\ &= \frac{-\int_0^t (\Gamma_L + \Gamma_O) T' dt}{mC' + \int_0^t (B_L + B_O) C' dt} = \frac{-(\gamma_L + \gamma_O) T'}{C'(m + \beta_L + \beta_O)}. \end{aligned} \quad (15)$$

When the assumed linearity for Eq. (3) holds and $T^* = 0$, then $\hat{g}_E = g_E$. With the additional assumption ($T' = \alpha C'$) that temperature change is linearly related to CO_2 change, $\hat{g}_E = -(\gamma_L + \gamma_O)\alpha/(m + \beta_L + \beta_O)$ becomes identical to concentration-based gain g of Friedlingstein et al. (2003). All the terms of the atmospheric carbon budget, feedback parameters, and values of gain g_E at the time of CO_2 quadrupling are compared across models in section 4b.

3. Model descriptions

The primary features of the nine participating models are summarized in Table 1 and brief descriptions of their terrestrial and oceanic carbon cycle components are provided in appendix C. The eight participating comprehensive ESMs, in alphabetical order, are the 1) Beijing Climate Centre (BCC) BCC-CSM1, 2) Canadian Centre for Climate Modeling and Analysis (CCCma) CanESM2, 3) L'Institut Pierre-Simon Laplace (IPSL) IPSL-CM5A-LR, 4) Japan Agency for Marine-Earth Science and Technology (JAMSTEC) MIROC-ESM, 5) Max Planck Institute for Meteorology (MPI) MPI-ESM-LR, 6) National Center for Atmospheric Research (NCAR) CESM1-BGC, 7) Norwegian Climate Centre (NCC) NorESM-ME, and 8) Met Office (UKMO) HadGEM2-ES. The ninth participating model, the University of Victoria (UVic) UVic ESCM 2.9, is an EMIC. The land surface scheme and carbon cycle component in the CESM1-BGC and NorESM-ME models is the community land model (CLM4) (Lawrence et al. 2011) which includes a representation of the nitrogen cycle and its coupling to the terrestrial carbon budget. None of the other participating models includes coupling of terrestrial carbon and nitrogen cycles.

4. Results

a. Surface CO_2 fluxes and temperature change

Figure 1 displays the specified atmospheric CO_2 concentration and the model mean and the intermodel range for simulated temperature change and atmosphere–land and atmosphere–ocean CO_2 flux changes (after accounting for the control run drift) and their cumulative values for the fully, radiatively, and biogeochemically coupled simulations. Figure 2 displays the cumulative fluxes for the individual models. In Fig. 1b, the model mean temperature change at the end of the simulation in the fully coupled case ($T' = 4.76^\circ\text{C}$) is higher by 0.42°C than in the radiatively coupled case ($T' = 4.34^\circ\text{C}$). The net effect of CO_2 -driven biogeophysical processes, operating in the fully coupled simulation compared to the radiatively coupled simulation, is a modest additional

TABLE 1. Primary features of the physical atmosphere and ocean components, and land and ocean carbon cycle components of the nine participating models in this study.

Modeling group	BCC	CCCma	IPSL	JAMSTEC
ESM	BCC-CSM1.1	CanESM2	IPSL-CM5A-LR	MIROC-ESM
Model expansion	Beijing Climate Center, Climate System Model, 1-1	Canadian Earth System Model, version 2	L'Institut Pierre-Simon Laplace Coupled Model, version 5, coupled with Nucleus for European Modeling of the Ocean (NEMO), low resolution	Model for Interdisciplinary Research on Climate, Earth System Model
Atmosphere resolution	~2.8°, L26	~2.8°, L35	3.75° × 1.90°, L39	T42, L80
Ocean resolution	0.3°–1.0° (zonal) × 1° (meridional), L40	1.41° × 0.94°, L40	2° (zonal) × 0.5°–2° (meridional), L31	~1.5°, L80
Land carbon cycle component				
Model name	BCC-AVIM1.0	CTEM	ORCHIDEE	SEIB-DGVM
Model expansion	Beijing Climate Center Atmosphere Vegetation Interaction Model Version 1.0	Canadian Terrestrial Ecosystem Model	Organizing Carbon and Hydrology in Dynamic Ecosystems	Spatially Explicit Individual-Based Dynamic Global Vegetation Model
No. of live and dead carbon pools	3	5	7	6
No. of PFTs	15	9	13	13
Fire	No	No	Yes	No
Dynamic vegetation cover	No	No	No	Yes
Nitrogen cycle	No	No	No	No
Ocean carbon cycle component				
Model name	OCMIP 2	CMOC	PISCES	NPZD
Model expansion	Ocean Carbon-Cycle Model Intercomparison Project Phase 2	Canadian Model of Ocean Carbon	Pelagic Interactive Scheme for Carbon and Ecosystem Studies	nutrient–phytoplankton–zooplankton–detritus
No. of phytoplankton types	—	1	2	1
No. of zooplankton types	—	1	2	1
Explicit nutrients	—	Nitrogen	Nitrogen, silica, phosphorus, iron	Nitrogen
Reference	Wu et al. 2013	Arora et al. 2011	Dufresne et al. 2013	Watanabe et al. 2011

warming. This warming is similar to that in the biogeochemically coupled simulation ($T^* = 0.32^\circ\text{C}$). The model-average temperature changes from the radiatively and biogeochemically coupled simulations add more or less linearly to that in the fully coupled simulation: that is, $T' \approx T^+ + T^*$ (4.76°C versus 4.66°C).

The modest increase in T^* in the biogeochemically coupled simulations is presumably due to a number of changes, including a reduction in transpiration due to increase in atmospheric CO_2 concentration, associated

with reduction in stomatal conductance (Boucher et al. 2009); an increase in vegetation leaf area index that decreases surface albedo, especially at high latitudes; and an increase in the fractional coverage of vegetation due to increasing CO_2 [in models that explicitly create competition between plant functional types (PFTs)], which decreases the surface albedo leading to more absorbed radiation and potentially reduces dust emissions (only the HadGEM2-ES and MIROC-ESM models include interactive dust emissions). Ocean

TABLE 1. (*Extended*)

UKMO	MPI	UVic	NCC	NSF-DOE-NCAR
HadGEM2-ES Hadley Centre Global Environmental Model 2, Earth System	MPI-ESM-LR Max Planck Institute Earth System Model, low resolution	UVic ESCM 2.9 University of Victoria Earth System Climate Model, version 2.9	NorESM-ME Norwegian Earth System Model (medium resolution)	CESM1-BGC Community Earth System Model, version 1.0, biogeochemical cycles
N96 ($1.25^\circ \times 1.875^\circ$), L38	$\sim 1.9^\circ$, L47	$3.6^\circ \times 1.8^\circ$, L1	$\sim 1.9^\circ \times 2.5^\circ$, L26	1.25° (zonal) $\times 0.94^\circ$ (meridional), L26
1° , L40	$\sim 1.5^\circ$, L47	$3.6^\circ \times 1.8^\circ$, L19	1° , L53	$\sim 1.12^\circ$ (zonal) \times 0.27° – 0.53° (meridional), L60
TRIFFID Top-down Representation of Interactive Foliage and Flora Including Dynamics	JSBACH Jena Scheme for Biosphere–Atmosphere Coupling in Hamburg	TRIFFID Top-down Representation of Interactive Foliage and Flora Including Dynamics	CLM4 Community Land Model, version 4	CLM4 Community Land Model, version 4
7	6	4	20	20
5	12	5	16	16
No	Yes	No	Yes	Yes
Yes	Yes	Yes	No	No
No	No	No	Yes	Yes
Diat-HadOCC Diatom Hadley Centre Ocean Carbon Cycle Model	HAMOCC Hamburg Model of the Ocean Carbon Cycle	2NZPD Two nutrient– zooplankton– phytoplankton– detritus	HAMOCC Hamburg Model of the Ocean Carbon Cycle	BEC Biogeochemical Elemental Recycling
3	1	2	2	3
1	1	1	1	1
Nitrogen, silica, iron Collins et al. 2011; Jones et al. 2011	Nitrogen, silica, phosphorus, iron Ilyina et al. 2013	Nitrogen, phosphorous Weaver et al. 2001; Eby et al. 2009	Nitrogen, phosphorous Tjiputra et al. (2013)	Nitrogen, silica, phosphorus, iron K. Lindsay et al. 2012, unpublished manuscript

accumulation of anthropogenic CO_2 can in principle also change ocean heat absorption by changing phytoplankton community structure and phytoplankton losses from the surface layer in sinking particles (by selecting against calcifying species and reducing availability of CaCO_3 as ballast), but this is a relatively minor effect and is not yet included in most models.

In the middle row of Fig. 1 the CO_2 flux from atmosphere to land and ocean in the biogeochemically coupled simulation (green lines) first increases and then

stays between 5 and 7 Pg C yr^{-1} (Figs. 1c,d). The carbon gains over land are a consequence of the CO_2 fertilization effect, which leads to increased gross primary productivity as well as the increase in the fractional coverage of vegetation (in models that model competition between PFTs). A higher concentration of atmospheric CO_2 increases the difference in CO_2 partial pressure between the atmosphere and the ocean, thereby driving the flux of CO_2 into the ocean. Carbon is lost to the atmosphere from both land and ocean in the radiatively

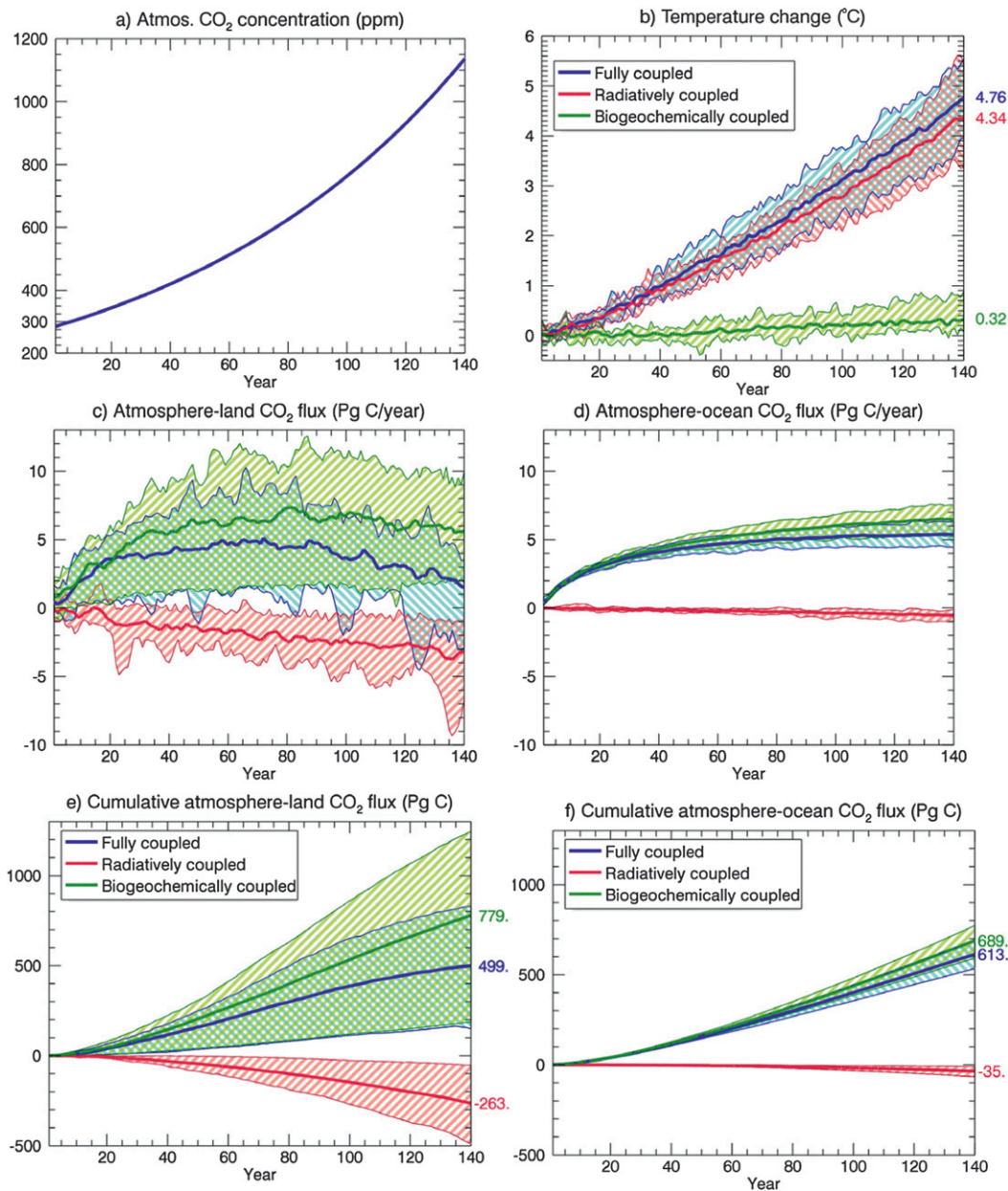


FIG. 1. (a) Atmospheric CO₂ concentration (ppm) used in the 1% increasing CO₂ simulations. (b) Model mean values and the range across the nine participating models for simulated temperature change, compared to the control simulation, (c) atmosphere-land and (d) atmosphere-ocean CO₂ fluxes, and (e), (f) their cumulative values, from the fully, radiatively, and biogeochemically coupled simulations.

coupled simulation. Over land temperature increase promotes increased heterotrophic respiration per unit biomass as well as decreased globally averaged net primary productivity (NPP) (not shown). Regionally, however, temperature increase is expected to enhance mid- to high-latitude primary production (Qian et al. 2010), so the reduction in global NPP is expected to come from the reduction in the tropics. Over the ocean, CO₂ loss is

associated with warmer temperatures, which reduce CO₂ solubility (Goodwin and Lenton 2009).

In Fig. 2, NorESM-ME and CESM1-BGC behave somewhat differently than the other models. Over land, they give up the lowest amount of carbon in response to warming in the radiatively coupled simulation (F_L^+ in Fig. 2e) but also take up the least amount of carbon in the biogeochemically coupled simulation in response

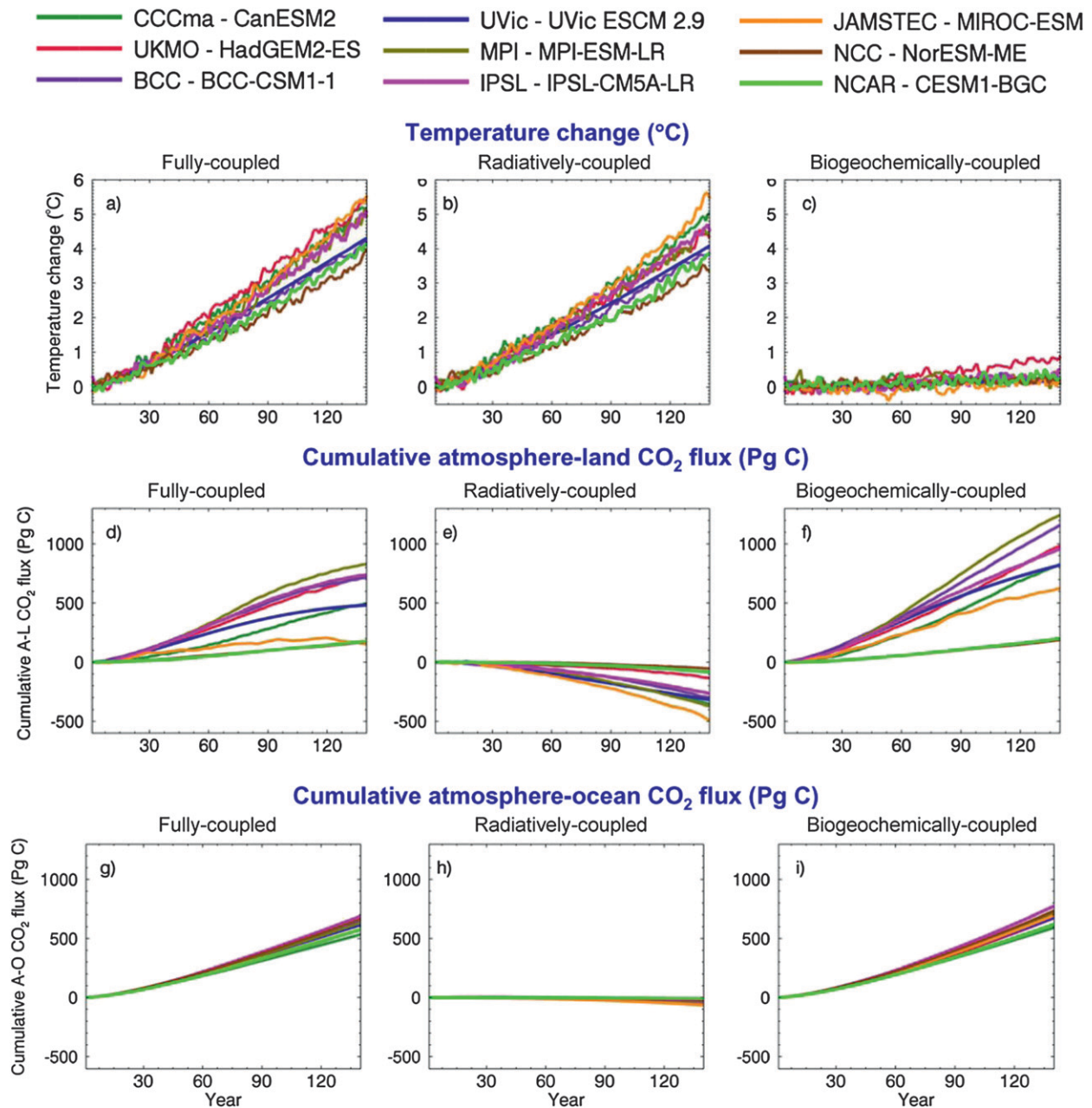


FIG. 2. (a)–(c) Simulated temperature change, (d)–(f) cumulative atmosphere–land CO₂ flux, and (g)–(i) cumulative atmosphere–ocean CO₂ flux from the fully, radiatively, and biogeochemically coupled 1% CO₂ increase simulations for the nine participating models. Note that in (d)–(f) the lines corresponding to the NorESM-ME and CESM1-BGC models essentially overlay each other.

to CO₂ increase (F_L^* in Fig. 2f). The overall result in the fully coupled simulation F_L' is also the smallest in Fig. 2d. The muted response of the land carbon cycle component (CLM4) of the NorESM-ME and CESM1-BGC models to increases in CO₂ concentration and temperature is not unexpected. The coupling of the carbon and nitrogen cycles reduces the CO₂ fertilization effect due to nitrogen limitation so the response to increased

CO₂ concentration in both models is lower than other models (Thornton et al. 2009; Bonan and Levis 2010). An interactive nitrogen cycle also counteracts increased ecosystem respiration losses and reduced productivity associated with temperature increase through carbon gains associated with more available mineral nitrogen. Other models that include coupling of terrestrial carbon and nitrogen cycles find similar behavior (Zaehle

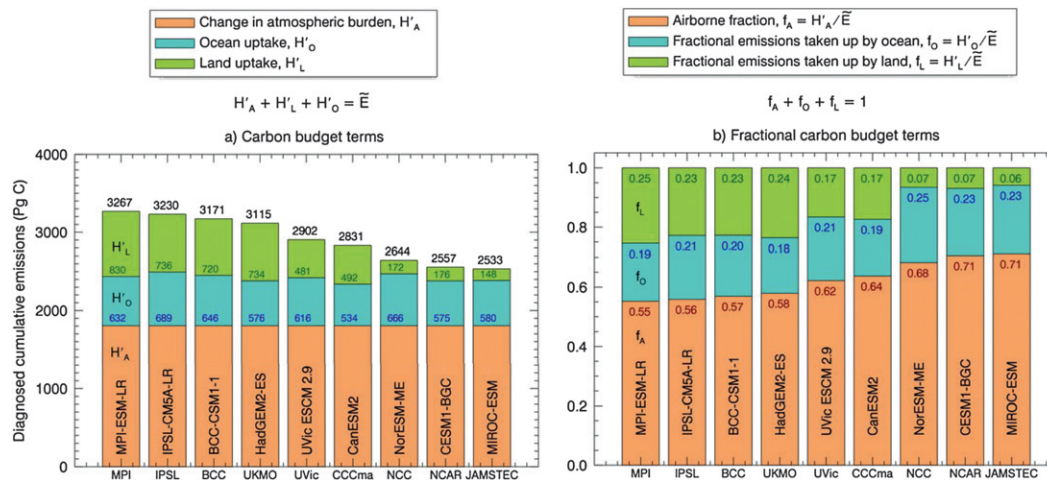


FIG. 3. Components of the atmospheric carbon budget of the participating nine models based on (a) Eq. (7) and (b) Eq. (10) using results from the fully coupled $1\% \text{ yr}^{-1}$ increasing CO_2 simulation. The terms are based on cumulative fluxes at the time of CO_2 quadrupling 140 yr after the start of the simulation. The models are arranged in a descending order based on their cumulative emissions values. In panel (a) carbon uptake by land and ocean components and diagnosed cumulative emissions and in panel (b) the airborne fraction and fraction of emissions taken up by land and ocean are also noted for individual models.

et al. 2010; Zhang et al. 2011). The range in cumulative atmosphere–surface CO_2 flux change among models, in response to changes in atmospheric CO_2 concentration and surface temperature (Figs. 1e,f), is 3–4 times larger at the end of the simulation for the land than for the ocean.

b. Cumulative emissions

Figure 3 displays atmospheric carbon budget components in Eqs. (7) and (10) using results from the fully coupled simulation. The results are arranged in descending order according to the models' cumulative emissions. The change in atmospheric carbon burden H'_A is specified in the $1\% \text{ CO}_2$ simulations so the differences in diagnosed cumulative emissions and its airborne fraction f_A are determined by land plus ocean carbon uptake in the models. Consistent with Figs. 1 and 2, the differences among models are primarily due to the diverse response of the land carbon cycle components (Fig. 3a).

c. Feedback parameters

1) CARBON–CONCENTRATION FEEDBACK PARAMETER

Figure 4 compares the atmosphere, land, and ocean carbon–concentration feedback parameters (B_A, B_L, B_O) across the nine models as a function of atmospheric CO_2 concentration calculated using results from the radiatively and biogeochemically coupled simulations (the R-B approach in appendix A). The feedback

parameters are calculated using 30-yr moving averaged atmosphere–surface CO_2 fluxes and the first 20 yr of data are not included in the plots so the CO_2 concentration along the x axis starts at 350 ppm. The plots are broadly similar when B is plotted against time since CO_2 increases monotonically (Fig. 1a). The terms B_L and B_O are positive, because higher CO_2 concentration results in flux into land and ocean carbon pools, while B_A is negative because the flux is out of the atmosphere. Both B_L and B_O decrease with increasing CO_2 for all models. For land F_L approaches a value between 5 and 7 Pg C (Fig. 1c) despite increasing CO_2 consistent with a decrease in the carbon–concentration feedback B_L . This is the consequence of increasing ecosystem respiration losses as total biomass increases as well as the saturation of the CO_2 fertilization effect with increasing CO_2 [e.g., see Luo et al. (1996) and Fig. 3c in Arora et al. (2009)]. Here, $B_L \approx F_L^*/C'$ [for small T^* from Eq. (4b)]; since C' is specified, the intermodel differences in B_L are the consequence of intermodel differences in the fluxes. The lowest value of B_L in the NorESM-ME and CESM1-BGC models are consistent with their nitrogen constraints on terrestrial photosynthesis, which reduces the strength of their CO_2 fertilization effect (Thornton et al. 2009; Bonan and Levis 2010).

For the oceans F_O approaches a constant value (Fig. 1d) associated with a decrease in B_O , with increasing CO_2 , as a consequence of the transport of carbon from the surface to the deep ocean failing to match the rate of increasing atmospheric CO_2 . As well, the ocean's buffering capacity declines, leaving a greater

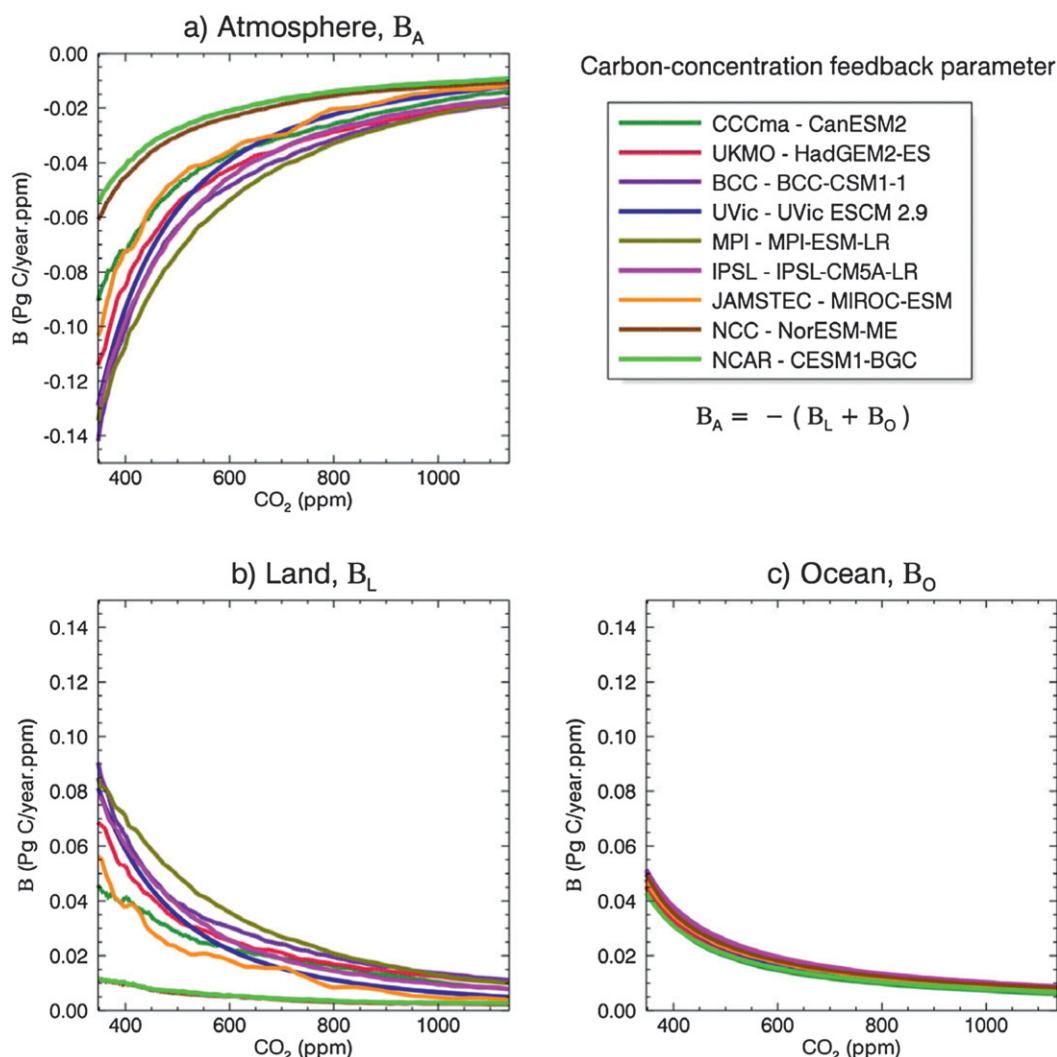


FIG. 4. Comparison of the carbon-concentration feedback parameter, calculated using the BA approach, across the nine participating models for the (a) atmosphere, (b) land, and (c) ocean components (B_i , $i = A, O, L$) plotted as a function of atmospheric CO_2 concentration.

fraction of anthropogenic carbon as CO_2 (instead of carbonate and bicarbonate ions). The B_O values are generally similar across the nine models because of relatively similar descriptions of the inorganic carbon cycle and gaseous CO_2 exchange. The B_L values, by contrast, show a wide range across the models.

2) CARBON-CLIMATE FEEDBACK PARAMETER

Figure 5 compares the atmosphere, land, and ocean carbon-climate feedback parameters ($\Gamma_A, \Gamma_L, \Gamma_O$) across the nine models as a function of global mean surface temperature change in the radiatively coupled simulation. The Γ values for the land and ocean are negative, because higher temperatures promote fluxes out of these components, and positive for the atmosphere because

the flux is into the atmosphere. Here Γ_L is larger than Γ_O so that for every 1°C increase in global temperature the land loses more carbon than the ocean. Values of Γ_L are negative on the global average because of increased ecosystem respiration per unit biomass as temperature increases as well as reduced photosynthesis. The land carbon cycle component in the NorESM-ME and CESM1-BGC models, which couple carbon and nitrogen cycles, has the lowest sensitivity to temperature change. These models lose less CO_2 than other models because the enhanced nitrogen mineralization, which accompanies temperature increase, enhances photosynthesis, which compensates for other losses. The reduced sensitivity of these models to temperature is consistent with other models that include coupled

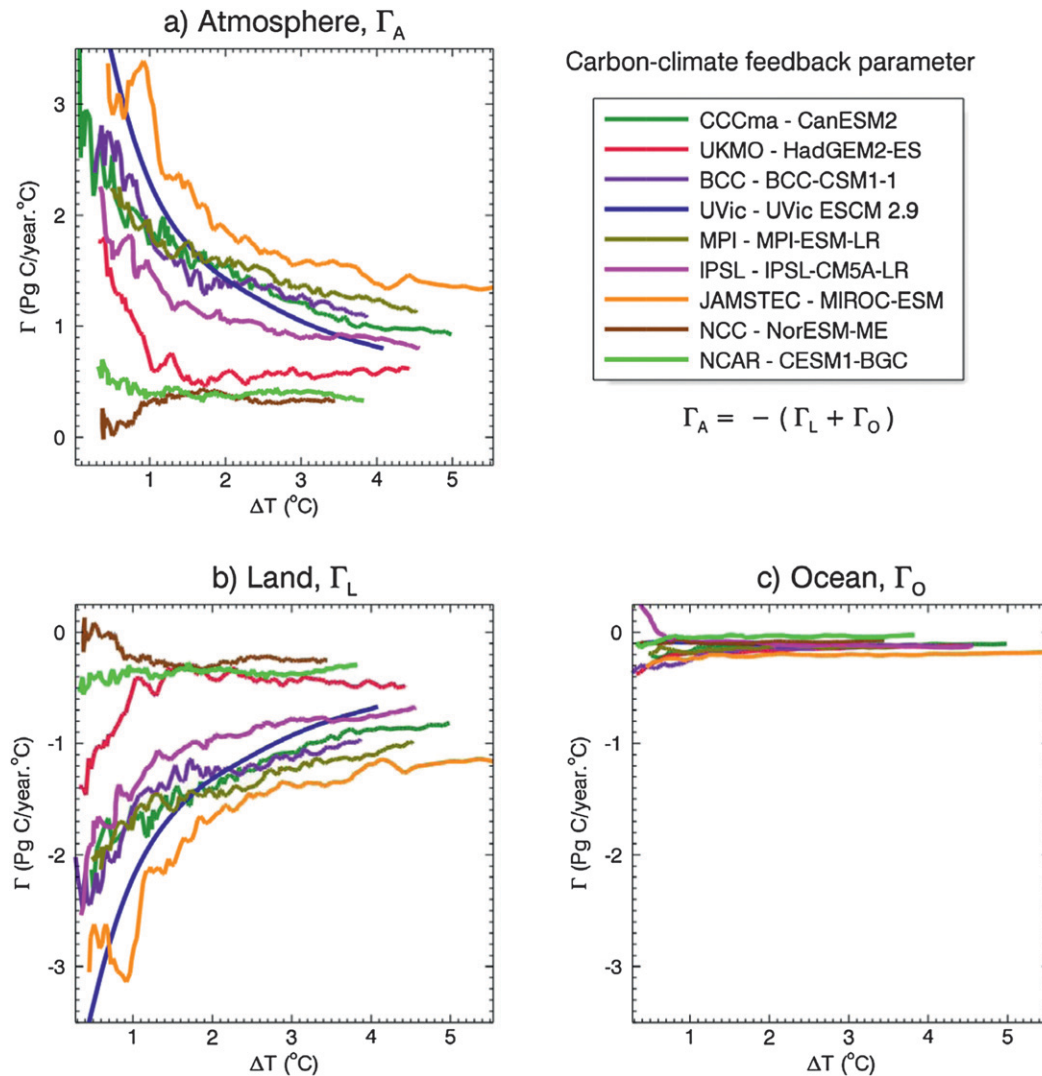


FIG. 5. Comparison of carbon-climate feedback parameter, calculated using the BA approach, across the nine participating models for the (a) atmosphere, (b) land, and (c) ocean components (Γ_i , $i = A, O, L$) plotted as a function of global mean surface temperature change in the radiatively coupled simulation.

terrestrial carbon and nitrogen cycles, although this reduction varies across models (Thornton et al. 2009; Zhang et al. 2011; Zaehle et al. 2010).

Increasing temperature leads to an increase in ecosystem respiration per unit biomass, but the absolute magnitude of Γ_L decreases with increasing temperature. This is because ecosystem respiration depends on both temperature and the respiring biomass. In the radiatively coupled simulations used to calculate Γ_L , the increase in temperature results in decreasing values of globally integrated vegetation and soil carbon mass (not shown) and this more than compensates for increasing respiration per unit biomass. This is one reason why feedback parameters are state dependent: in this case, due to the amount of land carbon.

The value of Γ_O is similar across models and only a weak function of temperature change. Warmer ocean temperatures reduce the solubility of CO_2 (Weiss 1974), but this reduction is a weak function of temperature (Heinze et al. 2003; Broecker and Peng 1986). The result is that the intermodel differences in Γ_A (Fig. 5a) and its overall behavior are almost entirely dominated by the response of the land carbon cycle components.

The first-order temperature control on ocean-atmosphere CO_2 flux is via the solubility of CO_2 in seawater, but this varies little among models as seen in Fig. 5c. Additional controls from ocean stratification, circulation, and biology are also part of the temperature- CO_2 flux feedback and are generally of the same sign (e.g., warmer, more stratified oceans generally have

less vertical flux of carbon into the surface layer). Biologically mediated fluxes affect physical transport (e.g., greater upward mixing flux of carbon is accompanied by greater downward flux of biogenic particles) but do not normally change the sign of the air–sea flux response. However, these processes are much more variable among models than the effect of temperature on solubility. For example, one model has a feedback parameter of opposite sign to the others for small temperature perturbations (Fig. 5c). This may also be in part due to weak temperature forcing early on in the radiatively coupled $1\% \text{ yr}^{-1}$ increasing CO_2 experiment.

3) INTEGRATED FLUX-BASED FEEDBACK PARAMETERS

Figure 6 displays the carbon–concentration (β_A , β_L , and β_O) and carbon–climate (γ_A , γ_L , and γ_O) feedback parameters calculated using the FEA and the R-B approaches. Models with higher (lower) values of B and Γ also have higher (lower) values of β and γ , and so the BA and FEA approaches agree to this extent. However, β does not display the monotonic behavior of B in Fig. 4 and its absolute values first increases and then decreases with increasing CO_2 . The absolute value of $\beta \approx \int_0^t F^* dt/C'$ increases (decreases) when the cumulative flux increases faster (slower) than the CO_2 concentration. For instance, increasing values of β_L (Fig. 6b) in the early part of the simulation result because of increasing F_L associated with increase in gross primary productivity due to the CO_2 fertilization effect and also expansion of vegetation in models that simulate competition between its PFTs. However, as ecosystem respiratory fluxes increase (due to increasing biomass), the rate of increase of F_L reduces and β_L begins to decrease. The β_O (Fig. 6b) shows a similar behavior but with a smaller change in its values.

The behavior of $\gamma_L = \int_0^t F_L^+ dt/T^+$ and $\gamma_O = \int_0^t F_O^+ dt/T^+$ in Figs. 6e and 6f is similarly explained. For both the land and ocean, the magnitude of cumulative atmosphere–surface CO_2 flux (in the radiatively coupled simulation) increases at a faster rate than the temperature, so the absolute values of γ_L and γ_O increase. Since the flux is out of the land and ocean carbon pools (i.e., negative F_L^+ and F_O^+), γ_L and γ_O are negative. Atmosphere–ocean CO_2 flux F_O^+ is not extremely sensitive to increases in temperature (as also seen for Γ_O in Fig. 5c) so the magnitude of γ_O increases only marginally. The magnitude of γ_L increases, with increasing temperature, despite decreasing absolute values of Γ_L (Fig. 4b), results because decreasing values of Γ_L are multiplied with increasing values of temperature change [Eq. (6a)] occurring over a larger fraction of land as the climate warms.

The BA and FEA approaches represent the coupled carbon–climate system feedbacks in different ways. In the BA approach, the feedback parameters represent the response of instantaneous fluxes to changes in CO_2 concentration and temperature, and negative and positive surface–atmosphere CO_2 fluxes lead to negative and positive feedbacks, respectively. The FEA approach represents the integrated response of the system, and negative and positive fluxes do not necessarily result in feedback parameters of the same sign.

Table 2 gives the integrated flux-based values of feedback parameters (β and γ), calculated at the end of the simulation, for the participating models together with the model-average values and their standard deviation, for the atmosphere, land, and ocean components. These may be compared with model average and standard deviation of the feedback parameters from the C⁴MIP study (Friedlingstein et al. 2006) for the A2 scenario, with the caveat that the feedback parameters are dependent on the scenario used and the approach used to calculate them. The results show that the strength of the feedbacks is weaker and the spread between models is smaller in this study. Excluding results from the NorESM-ME and CESM1-BGC models still yields weaker strength of the feedbacks and a smaller spread than the C⁴MIP study (not shown). The spread between the feedback parameters is particularly smaller for the ocean carbon cycle component compared to the C⁴MIP study.

4) FEEDBACK CONTRIBUTIONS

The relative contributions of the carbon–concentration and carbon–climate feedbacks to the carbon budget can be quantified following Eqs. (8) and (11) provided the surface–atmosphere flux in the fully coupled simulation can be represented in terms of feedback parameters with $F_A' \approx B_A C' + \Gamma_A T'$ as shown in appendix B. (Figure B1 shows that this is generally the case, and Fig. 7 displays these contributions.)

Figure 7 displays cumulative emissions ($H_A' + H_C' + H_T' \approx \bar{E}$), consistent with the $1\% \text{ yr}^{-1}$ increasing CO_2 scenario, in terms of the change in the atmospheric burden and the contributions of the feedbacks following Eqs. (8) and (11). The effect of carbon–concentration feedback H_C' is positive indicating uptake of emitted CO_2 . By contrast, the effect of carbon–climate feedback H_T' is negative indicating a release of CO_2 , which partially offsets H_C' . The net magnitude of the feedbacks varies appreciably across models. The average across nine models for H_C' is 1450 with an intermodel standard deviation of 385 Pg C. The corresponding mean and standard deviation values for H_T' are -314 and 159 Pg C. The land and ocean contributions of the feedbacks to the

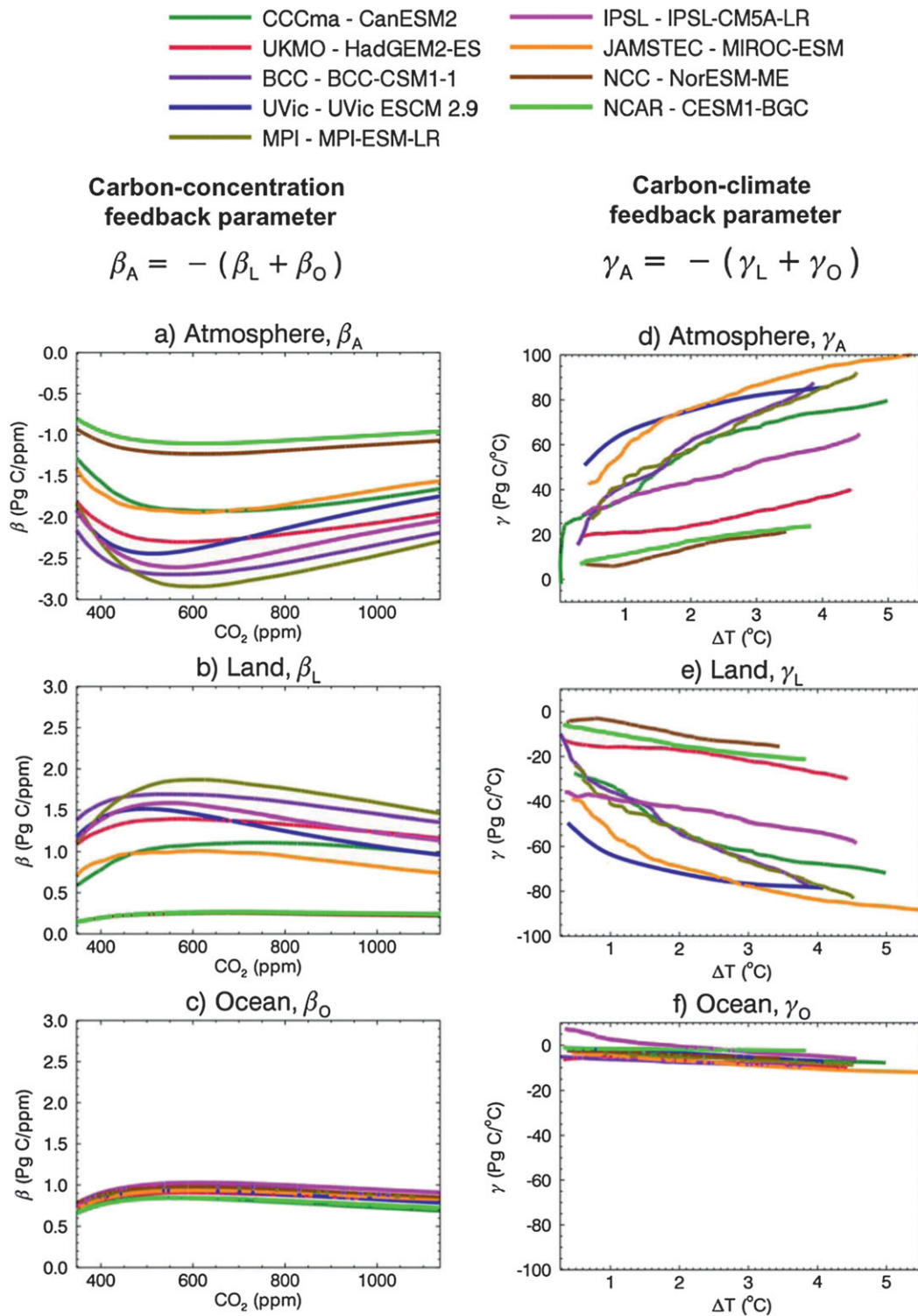


FIG. 6. Comparison of the integrated flux-based carbon-concentration (β_A , β_L , and β_O) and carbon-climate (γ_A , γ_L , and γ_O) feedback parameters across the nine participating models for the (a),(d) atmosphere; (b),(e) land; and (c),(f) ocean components.

TABLE 2. Values of integrated flux-based carbon–concentration β and carbon–climate γ feedback parameters for the participating models for their atmosphere, land, and ocean components calculated using data at the end of the radiatively and biogeochemically coupled simulations.

Model	Carbon–concentration feedback parameter β (Pg C ppm ^{−1})			Carbon–climate feedback parameter γ (Pg C °C ^{−1})		
	β_A Atmosphere	β_L Land	β_O Ocean	γ_A Atmosphere	γ_L Land	γ_O Ocean
MPI-ESM-LR	−2.29	1.46	0.83	92.2	−83.2	−9.0
IPSL-CM5A-LR	−2.04	1.14	0.91	64.8	−58.6	−6.2
BCC-CSM1	−2.19	1.36	0.83	87.6	−77.8	−9.8
HadGEM2	−1.95	1.16	0.79	40.1	−30.1	−10.0
UVic ESCM 2.9	−1.75	0.96	0.78	85.8	−78.5	−7.3
CanESM2	−1.65	0.97	0.69	79.7	−71.9	−7.8
NorESM-ME	−1.07	0.22	0.85	21.4	−15.6	−5.7
CESM1-BGC	−0.96	0.24	0.72	23.8	−21.3	−2.4
MIROC-ESM	−1.56	0.74	0.82	100.7	−88.6	−12.1
Model mean (std dev)	−1.72 (0.47)	0.92 (0.44)	0.80 (0.07)	66.2 (30.4)	−58.4 (28.5)	−7.8 (2.9)
C ⁴ MIP mean (std dev) (FEA)	−2.48 (0.59)	1.35 (0.61)	1.13 (0.26)	109.6 (50.6)	−78.6 (45.8)	−30.9 (16.3)

atmospheric carbon budget, based on Eqs. (9) and (11), are shown in Fig. 8. The effect of the ocean carbon–climate feedback on the overall atmospheric carbon budget is small. Both carbon–concentration and carbon–climate feedbacks over ocean vary little between models. For all models, except NorESM-ME and CESM1-BGC, the land carbon cycle component dominates the overall carbon–climate feedback.

Figures 7 and 8 show that, because of their offsetting nature, similar values of cumulative emissions and airborne fractions result even though the strength of feedbacks vary considerably across models. The higher airborne fraction of cumulative emissions in the CanESM2, NorESM-ME, CESM1-BGC, and MIROC-ESM models

(0.64–0.71) is associated with their relatively smaller fraction of emissions taken up by land (0.06–0.17), compared to other comprehensive Earth system models. This is related to a weaker CO₂ fertilization effect in these models. In the absence of an explicit terrestrial nitrogen cycle, the strength of the CO₂ fertilization effect in CanESM2 is “downregulated” based on the response of plants grown in ambient and elevated CO₂ following Arora et al. (2009). The CO₂ fertilization effect in the NorESM-ME and CESM1-BGC models is constrained by nitrogen limitation. Finally, unlike other models, which use a biogeochemical approach to model terrestrial photosynthesis, the MIROC-ESM uses an empirical approach to model the photosynthetic response

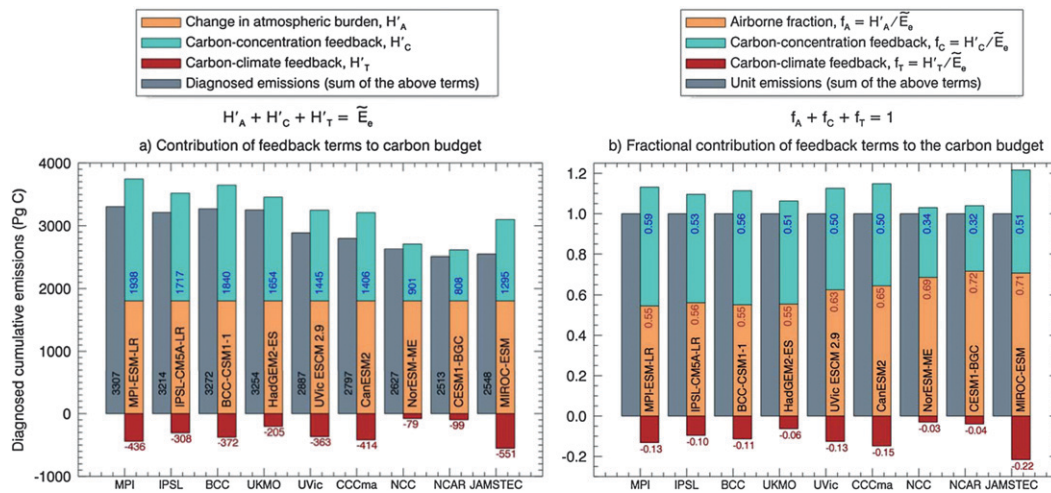


FIG. 7. Contributions of the carbon–concentration and carbon–climate feedbacks to the emissions carbon budget (a) in terms of their absolute magnitudes and (b) as a fraction of cumulative emissions following Eqs. (8) and (11).

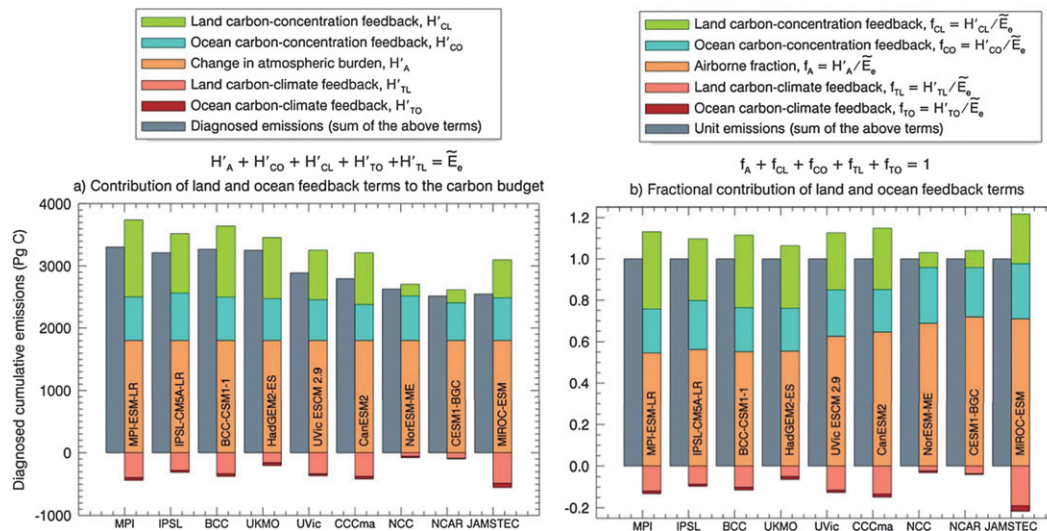


FIG. 8. Land and ocean contributions of the carbon–concentration and carbon–climate feedbacks to the atmospheric carbon budget (a) in terms of their absolute magnitudes and (b) also as a fraction of cumulative emissions following Eqs. (9) and (11).

to CO_2 (Ito and Oikawa 2002), which implicitly includes the response to nutrient limitation.

5) GAIN

Gain g_E [Eq. (13)] quantifies the increase in cumulative emissions when carbon–climate feedback is absent (see section 2d) and is compared across the nine models in Fig. 9. The \hat{g}_E compares relatively well with g_E , for seven of the nine models considered, implying that feedback parameters may be used to quantify the carbon–climate feedback in terms of gain for most models. The \hat{g}_E does not compare well with g_E for the BCC-CSM1.1 and HadGEM2-ES models, for which the conditions $F' = F^+ + F^*$ and $T' = T^+ + T^*$ are not met as well as for other models (see Fig. B1b). In addition, the HadGEM2-ES model shows the largest warming in the biogeochemically coupled case (Fig. 2c), so the approximation $T^* \approx 0$ in Eq. (15) is not satisfied. Higher (lower) values of g_E values imply a larger (smaller) contribution of carbon–climate feedback to the atmospheric carbon budget.

5. Summary and conclusions

Results from biogeochemically, radiatively, and fully coupled simulations in which CO_2 increases at a rate of $1\% \text{ yr}^{-1}$ until values quadruple after 140 years are analyzed. In the biogeochemically coupled simulations, all biogeochemical processes are active but the specified increasing CO_2 concentration changes are excluded from the model's radiation code. In the radiatively coupled

simulations the model's radiation code responds to specified increases in atmospheric CO_2 concentration, but the biogeochemistry components see the preindustrial value. These simulations isolate the system's response to changes in temperature and CO_2 concentration. In the fully coupled simulation, all processes are active.

Two approaches are used to characterize the behavior of the coupled carbon–climate system in terms of feedback parameters. In the first approach, carbon–climate (Γ ; $\text{Pg C yr}^{-1} \text{ } ^\circ\text{C}^{-1}$) and carbon–concentration (B ; $\text{Pg C yr}^{-1} \text{ ppm}^{-1}$) feedback parameters are obtained following Boer and Arora (2009, 2010) in which atmosphere–surface CO_2 flux changes, from a control simulation, are expressed in terms of temperature and CO_2 concentration changes. The feedback parameters in

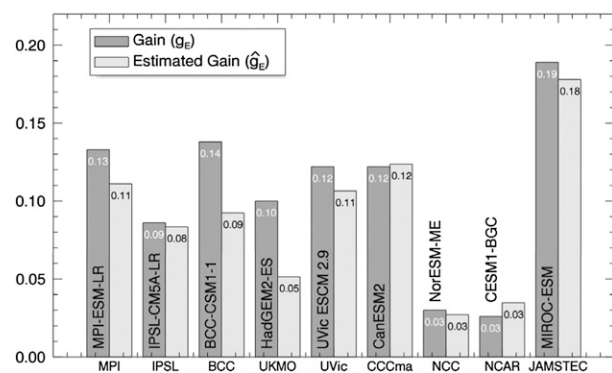


FIG. 9. Gain g_E [Eq. (13)] and its estimated value based on feedback parameters \hat{g}_E [Eq. (15)] for the nine participating models.

this approach represent the averaged partial derivative of CO_2 fluxes with respect to temperature and CO_2 concentration. The second approach follows Friedlingstein et al. (2006) and others (Gregory et al. 2009; Roy et al. 2011) in which integrated flux changes up to a given point in time (i.e., changes in pool sizes) are expressed in terms of temperature and CO_2 concentration changes to obtain carbon–climate (γ ; $\text{Pg}^\circ\text{C}^{-1}$) and carbon–concentration (β ; Pg C ppm^{-1}) feedback parameters.

Carbon–concentration feedback is negative from the atmosphere’s perspective and quantifies the loss of CO_2 to the land and ocean as atmospheric CO_2 concentration increases. The carbon–climate feedback parameter is positive from the atmosphere’s perspective because both the land and ocean give up carbon in response to temperature increases. In all models, the magnitude of B decreases for both the land and the ocean as CO_2 increases. Over the land, this is related to the saturation of the CO_2 fertilization effect and increased ecosystem respiration fluxes as vegetation and soil carbon biomass increase. Over the ocean decreasing values of B result because the transport of CO_2 to the deep ocean limits the ocean uptake of CO_2 . The B values are generally similar over the land and ocean but with a wider range among models for land carbon cycle components. The magnitude of Γ for land also decreases with increasing temperature. For the ocean, Γ is a weak function of temperature change. The values of Γ for the land are generally an order of magnitude larger than for the ocean, and the positive carbon–climate feedback is dominated by the behavior of the terrestrial ecosystems.

The intermodel range in both feedback parameters is larger for land than for the ocean, and on a global scale the differences in carbon feedbacks among ESMs are dominated by the diverse response of the land carbon cycle components in the participating models. This agrees with results from the Coupled Climate Carbon Cycle Model Intercomparison (C^4MIP) of Friedlingstein et al. (2006). The physical and chemical processes that determine CO_2 uptake in the ocean at the time scales considered here are generally similar across the models. The spread in the integrated flux-based feedback parameters for the ocean component is much smaller in CMIP5 models considered here than in the C^4MIP study (Table 2), with the caveat that a different scenario and approach is used here to calculate feedback parameters.

The contribution of carbon–concentration feedback to diagnosed cumulative emissions, for the 1% increasing CO_2 specified concentration simulations analyzed here, is about 4.5 times larger than the carbon–climate feedback. Analogous to gain g that quantifies the relative

increase in atmospheric CO_2 concentration associated with carbon–climate feedback, gain g_E quantifies the increase in implied emissions when the carbon–climate feedback is absent. Gain g_E is lowest for the NorESM-ME and CESM1-BGC models, which both have a weak carbon–climate feedback. These are the only participating models that include coupled terrestrial carbon and nitrogen cycles, which also have an overall weak carbon–concentration feedback (due to their weaker land carbon–concentration feedback associated with nitrogen constraints on terrestrial photosynthesis). The lower value of Γ_L and g_E in the NorESM-ME and CESM1-BGC models, compared to other models, indicates that positive carbon–climate feedback over land may be much weaker than previously thought, although much uncertainty remains (Zaehle et al. 2010; Zhang et al. 2011) and none of the CMIP5 models includes the positive permafrost–carbon feedback (MacDougall et al. 2012). While γ_L is small and negative for both NorESM-ME and CESM1-BGC models (Table 2), simulations with an earlier version of the same land model (CLM4) reported a small positive value (Thornton et al. 2009).

The feedback parameters characterize broad features of system behavior, but they are dependent on the state of the system, the forcing scenario, and the approach used to calculate them, implying that flux changes cannot be characterized solely in terms of linear responses of temperature and CO_2 concentration changes. Despite this state dependence, however, the feedback parameters provide insight into the behavior of feedbacks operating in the coupled carbon–climate system and provide a useful common framework for comparing models.

Acknowledgments. We acknowledge the World Climate Research Programme’s Working Group on Coupled Modelling, which is responsible for CMIP, and we thank the climate modeling groups (listed in Table 1 of this paper) for producing and making available their model output. For CMIP, the U.S. Department of Energy’s Program for Climate Model Diagnosis and Intercomparison provides coordinating support and led development of software infrastructure in partnership with the Global Organization for Earth System Science Portals. CDJ acknowledges U.K. government funding and was supported by the Joint DECC/Defra Met Office Hadley Centre Climate Programme (GA01101). Both CDJ and PF acknowledge the COMBINE EU project. JFT was supported by the Research Council of Norway through the EarthClim (207711/E10) project. Comments on an earlier version of this paper from Greg Flato and Nathan Gillett and two anonymous reviewers are also greatly appreciated.

APPENDIX A

Solving for Feedback Parameters

The set of Eqs. (3) for the direct/instantaneous feedback BA approach and Eq. (5) for the integrated flux-based FEA approach can be solved in three different ways to obtain values of Γ and B and of γ and β . The two feedback parameters can be calculated using results from the radiatively and biogeochemically coupled simulations [Eqs. (3a) and (3b): the R-B approach], the radiatively and fully coupled simulations [Eqs. (3a) and (3c): the R-F approach], or the biogeochemically and fully coupled simulations [Eqs. (3b) and (3c): the B-F approach]. The subscript A is omitted for clarity in the following:

- the R-B approach,

$$\Gamma = \frac{F^+}{T^+} \quad \text{and} \quad (A1a)$$

$$B = \frac{F^* - \Gamma T^*}{C'}; \quad (A1b)$$

- the R-F approach,

$$\hat{\Gamma} = \frac{F'}{T'} = \Gamma \quad \text{and} \quad (A2a)$$

$$\begin{aligned} \hat{B} &= \frac{F' - \Gamma T'}{C'} \\ &= B + \frac{(F' - F^*)}{C'} - \frac{\Gamma(T' - T^*)}{C'}; \quad \text{and} \\ &= B + \Delta\hat{B} \end{aligned} \quad (A2b)$$

- the B-F approach,

$$\begin{aligned} \tilde{\Gamma} &= \frac{F' - F^*}{T' - T^*} \\ &= \Gamma + \frac{(F' - F^*)T^+ - (T' - T^*)F^+}{(T' - T^*)T^+} \quad \text{and} \\ &= \Gamma + \Delta\tilde{\Gamma} \end{aligned} \quad (A3a)$$

$$\begin{aligned} \tilde{B} &= \frac{1}{C'} \left(\frac{F^*T' - F'T^*}{T' - T^*} \right) \\ &= B + \frac{1}{C'} \left(\Gamma T^* - \frac{(F' - F^*)T^*}{T' - T^*} \right) \\ &= B + \Delta\tilde{B}. \end{aligned} \quad (A3b)$$

In Eqs. (A1)–(A3), if the conditions $F' = F^+ + F^*$ and $T' = T^+ + T^*$ are met (i.e., if the sum of flux and temperature changes in the radiatively and biogeochemically coupled simulations is the same as that in the fully

coupled simulation), then all approaches yield exactly the same solution since $\Delta\hat{B}$, $\Delta\tilde{\Gamma}$, and $\Delta\tilde{B}$ all converge to zero.

These two conditions are not exactly satisfied for the participating models. Figure A1 shows that the calculated values of B , the carbon–concentration feedback parameter, using the three approaches are very similar, although the value of $\tilde{\Gamma}$ is somewhat different from that of Γ . That the value of Γ_i depends on the approach used is consistent with earlier results that the feedback parameters are scenario dependent or, more appropriately, state dependent (Boer and Arora 2009, 2010; Gregory et al. 2009; Zickfeld et al. 2011).

APPENDIX B

Cumulative Emissions

Figure B1a shows that the cumulative emissions from the fully coupled simulation [\tilde{E} ; Eq. (7)] are in good agreement with those calculated using the feedback parameters [$\tilde{E} + \delta\tilde{E}$; Eq. (8)], and the cumulative difference $\delta\tilde{E}$ is small compared to the cumulative flux $\int_0^t F'_A dt$ (Fig. B1b), except for the BCC-CSM1.1 and HadGEM2-ES models [as also found by Gregory et al. (2009) for the third-generation low-resolution Hadley Centre climate model with carbon cycle (HadCM3LC)]. The overall good agreement in Fig. B1a is the result of $F' = F^+ + F^*$ and $T' = T^+ + T^*$ conditions being met for most models indicating that feedback parameters calculated using results from radiatively and biogeochemically coupled simulations transfer well to the fully coupled case. Zickfeld et al. (2011) found that, for the concentration-driven simulations, with the UVic ESCM v2.9, the diagnosed emissions from the radiatively and biogeochemically coupled cases combined linearly to give diagnosed emissions from the fully coupled case up to around 2100 but not after that. Here, for the concentration-driven 1% increasing CO₂ scenario, the linearity assumption holds fairly well for the UVic ESMC v2.9.

APPENDIX C

Model Descriptions

a. Beijing Climate Centre CSM1

The Beijing Climate Centre (BCC) CSM1.1 is a fully coupled global climate–carbon model including interactive vegetation and global carbon cycle (Wu et al. 2013). The atmospheric component BCC-AGCM2.1 is a global spectral model with a horizontal resolution of

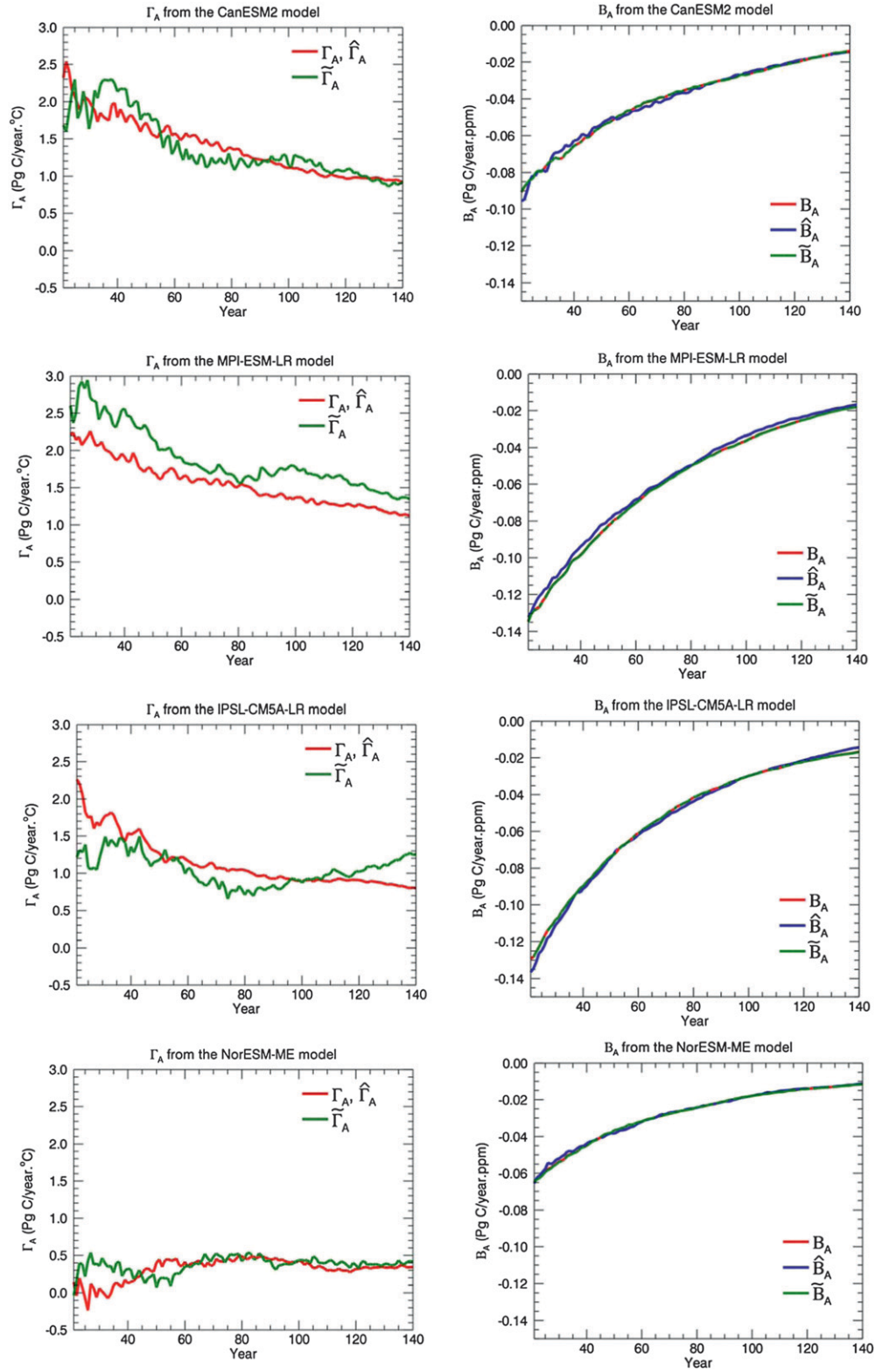


FIG. A1. Calculated values of Γ_A (carbon-climate) and B_A (carbon-concentration) feedback parameters for the four of the participating models using the three approaches illustrated in appendix A.

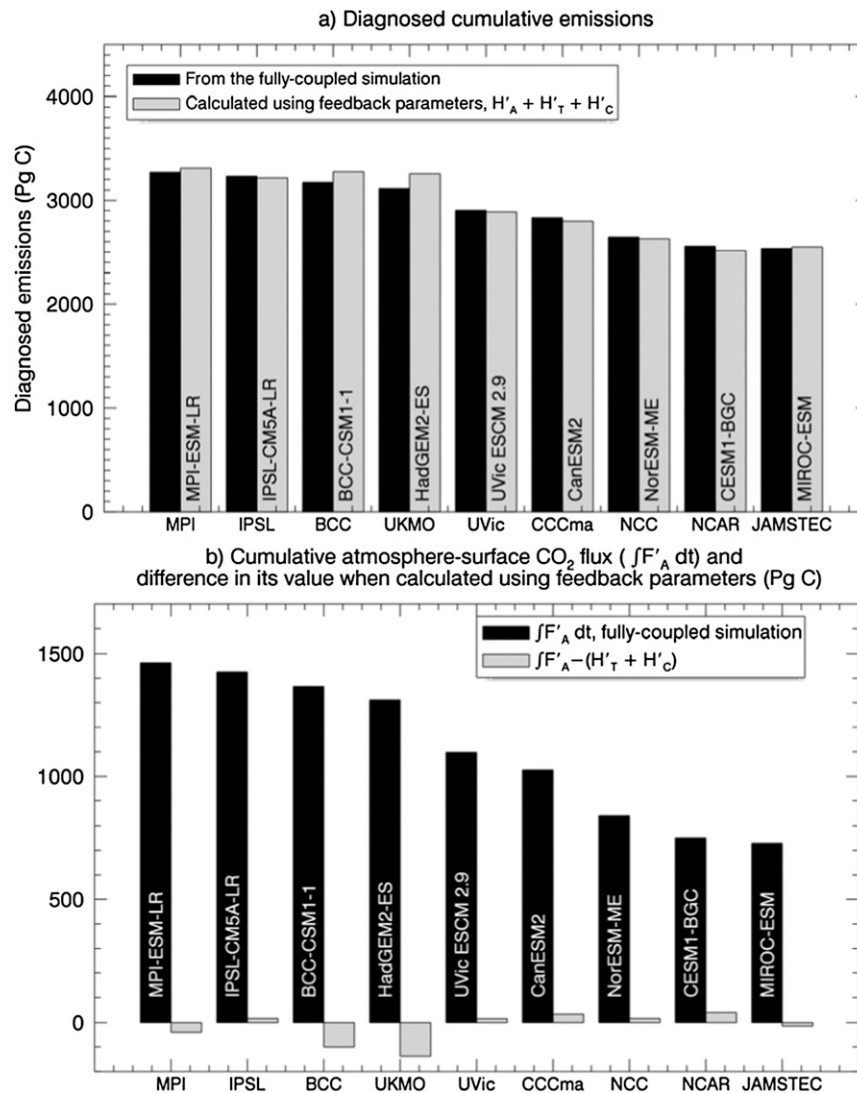


FIG. B1. (a) Comparison of diagnosed cumulative emissions from the fully coupled simulation \bar{E} to those estimated using $H'_A + H'_C + H'_T = \bar{E} + \delta\bar{E}$ [Eq. (8)]. The models are arranged in a descending order based on their cumulative emissions values. (b) Comparison of the difference in cumulative emissions $\delta\bar{E} = \int_0^t F'_A dt - (H'_C + H'_T)$ to $\int_0^t F'_A dt$ from the fully coupled simulation.

T42, approximately $2.81^\circ \times 2.81^\circ$ transformed grid, and 26 levels in a hybrid sigma/pressure vertical coordinate system with the top level at 2.91 hPa. The dynamical core of the model is described in Wu et al. (2008), a precedent version BCC-AGCM2.0 is detailed in Wu et al. (2010). A new deep convective scheme of Wu (2012) is used in BCC-AGCM2.1. The oceanic general circulation model (OGCM) Modular Ocean Model, version 4 (MOM4-L40) uses a tripolar grid of Murray (1996). The horizontal resolution is 1° longitude by $\frac{1}{3}^\circ$ latitude between 30°S and 30°N and increases to 1° at 60°N and beyond, and there are 40 z levels in the vertical.

It adopts some mature parameterization schemes used in MOM4 (Griffies et al. 2005), including Sweby's tracer-based third-order advection scheme, isopycnal tracer mixing and diffusion scheme, Laplace horizontal friction scheme, K -profile parameterization (KPP) vertical mixing scheme, complete convection scheme, overflow scheme of topographic processing of sea bottom boundary/steep slopes, and shortwave penetration schemes based on spatial distribution of chlorophyll concentration.

The terrestrial carbon cycle components are described in Ji et al. (2008) and models biochemical and physiological processes including photosynthesis and

respiration of vegetation; allocation of carbohydrate to leaves, stem, and root tissues; carbon loss due to turnover and mortality of vegetation; and CO₂ release into atmosphere through soil respiration. The model can treat 15 plant functional types (PFTs) including natural vegetation and crop and a grid cell can contain up to four PFTs.

The biogeochemistry module of MOM4-L40 is based on the protocols of the Ocean Carbon Cycle Model Intercomparison Project–Phase 2 (OCMIP2; <http://www.ipsl.jussieu.fr/OCMIP/phase2/>), which parameterizes the process of marine biology in terms of geochemical fluxes without explicit representation of the marine ecosystem and food web processes. It includes five prognostic variables: phosphate (PO₄), dissolved organic phosphorus (DOP), dissolved oxygen (O₂), dissolved inorganic carbon (DIC), and alkalinity (Alk). Export production (EP) is parameterized by restoring phosphate production to a climatological state (implicitly this eliminates possible feedbacks on productivity). In the oceanic component (MOM4_L40) of BCC-CSM1.1, the restoring EP has been replaced with a prognostic scheme following Yamanaka and Tajika (1996). EP in MOM4_L40 is parameterized as a function of phosphate concentration [PO₄], $EP = rL_f[PO_4]$, where r is a proportional factor called “bio-production efficiency” and is set to 0.8 yr^{-1} in MOM4_L40 and L_f is the light factor related to strength of the incident solar radiation (Bacastow and Maier-Reimer 1990).

b. Canadian Centre for Climate Modeling and Analysis CanESM2

CanESM2 has evolved from the first-generation Canadian Earth System Model (CanESM1) (Arora et al. 2009; Christian et al. 2010) of the Canadian Centre for Climate Modeling and Analysis (CCCma) and is described in Arora et al. (2011). The vertical domain of the atmospheric component of CanESM2 (CanAM4) extends to 1 hPa with the thicknesses of the model's 35 layers increasing monotonically with height. The physical ocean component of CanESM2 has 40 levels with approximately 10-m resolution in the upper ocean compared to 29 levels in CanESM1, providing a much improved representation of the euphotic zone. The ocean horizontal resolution is approximately 1.41° (longitude) \times 0.94° (latitude) in CanESM2.

The Canadian Model of Ocean Carbon (CMOC), the ocean carbon cycle component of CanESM2, incorporates an inorganic chemistry module (solubility pump) and a nutrient–phytoplankton–zooplankton–detritus (NPZD) ecosystem model (organic and carbonate pumps) for simulating the ocean–atmosphere exchange of CO₂ (Zahariev et al. 2008). Ocean chlorophyll (which affects

penetrating shortwave radiation and thus subsurface heating) is a “semi-prognostic” variable that evolves with time but is not advected independently of phytoplankton biomass. Terrestrial ecosystem processes are modeled using the Canadian Terrestrial Ecosystem Model (CTEM), which simulates carbon in three live vegetation pools (leaves, stem, and root) and two dead pools (litter and soil organic carbon) for nine PFTs: needleleaf evergreen and deciduous trees, broadleaf evergreen and cold and dry deciduous trees, and C₃ and C₄ crops and grasses. (Arora and Boer 2010).

c. L’Institut Pierre-Simon Laplace CM5A-LR

The IPSL-CM5A (Dufresne et al. 2013), is the new generation Earth system model developed at L’Institut Pierre-Simon Laplace (IPSL). The atmosphere and land models of IPSL-CM5 are updated versions of those used in IPSL-CM4 (Marti et al. 2010): namely, the Laboratoire de Météorologie Dynamique Model with Zoom Capability (LMDZ) atmospheric general circulation model (Hourdin et al. 2006) and the ORCHIDEE land surface model (Krinner et al. 2005). The atmospheric and land components use the same regular horizontal grid with 96×96 points, representing a resolution of $3.6^\circ \times 1.8^\circ$, while the atmosphere has 39 vertical levels. The oceanic component is NEMOv3.2 (Madec 2008), which includes the Louvain-la-Neuve sea ice model (LIM; Fichet and Morales Maqueda 1997) and the marine biogeochemistry model PISCES (Aumont and Bopp 2006). The ocean model has a horizontal resolution of 2° – 0.5° and 31 vertical levels.

The land carbon component ORCHIDEE (Krinner et al. 2005) simulates, with a daily time step, processes of photosynthesis, carbon allocation, litter decomposition, soil carbon dynamics, maintenance and growth respiration, and phenology for 13 different plant functional types. The ocean carbon component PISCES (Aumont and Bopp 2006) simulates the cycling of carbon, oxygen, and the major nutrients determining phytoplankton growth (phosphate, nitrate, ammonium, iron, and silicic acid). PISCES also includes a simple representation of the marine ecosystem with two phytoplankton and two zooplankton size classes.

d. Japan Agency for Marine-Earth Science and Technology MIROC-ESM

The MIROC-ESM (Watanabe et al. 2011) is based on the Model for Interdisciplinary Research on Climate (MIROC) global climate model (Nozawa et al. 2007), which interactively couples an atmospheric general circulation model (MIROC-AGCM; Watanabe et al. 2008), including an online aerosol component [Spectral Radiation-Transport Model for Aerosols Species

(SPRINTARS 5.00); Takemura et al. 2000], an ocean GCM with sea ice component [Center for Climate System Research (CCSR) Ocean Component Model (COCO); Hasumi 2007], and a land surface model [Minimal Advanced Treatments of Surface Interaction and Runoff (MATSIRO); Takata et al. 2003].

The MIROC-AGCM has a spectral dynamical core and uses a flux-form semi-Lagrangian scheme for the tracer advection. The grid resolution is approximately 2.81° with 80 vertical levels between the surface and about 0.003 hPa. The physical ocean component of MIROC-ESM (COCO 3.4) has longitudinal grid spacing of about 1.4° , while the latitudinal grid intervals gradually vary from 0.5° at the equator to 1.7° near the North/South Pole with 44 levels in the vertical.

MIROC-ESM includes an NPZD type of ocean ecosystem component (Oschlies 2001) and a terrestrial ecosystem component with dynamic vegetation (SEIB-DGVM; Sato et al. 2007). A version of the model that includes an atmospheric chemistry component [Clouds, Hazards, and Aerosols Survey for Earth Researchers (CHASER); Sudo et al. 2002] is called MIROC-ESM-CHEM but is not used here. MIROC-ESM includes an atmospheric chemistry component (CHASER 4.1), an NPZD-type ocean ecosystem component (Oschlies 2001), and a terrestrial ecosystem component with dynamic vegetation (SEIB-DGVM; Sato et al. 2007). The NPZD sufficiently resolves the seasonal variation of oceanic biological activities at a basinwide scale (Kawamiya et al. 2000). The biological primary production and NPZD variables are computed above the euphotic layer, in a nitrogen base. A constant Redfield ratio ($C/N = 6.625$) is used to estimate the carbon and calcium flow. The sea–air CO_2 flux is calculated by multiplying the difference of ocean–atmosphere CO_2 partial pressures by the ocean gas solubility. SEIB-DGVM adopts an individual-based simulation scheme that explicitly captures light competition among trees. Vegetation is classified into 13 PFTs, consisting of 11 tree PFTs and 2 grass PFTs. The dynamics of the two soil organic carbon pools (fast and slow decomposing) is based on the Roth-C scheme (Coleman and Jenkinson 1999).

e. Max Planck Institute for Meteorology ESM-LR

The Earth system model developed at the Max Planck Institute for Meteorology in Hamburg, Germany (MPI-ESM; Giorgetta et al. 2012, manuscript submitted to *J. Adv. Model. Earth Syst.*), consists of a general circulation model for the atmosphere (ECHAM6) (Stevens et al. 2013; Roeckner et al. 2003) at T63 ($1.9^\circ \times 1.9^\circ$) resolution with 47 vertical levels and the oceanic model MPI-OM with a nominal horizontal resolution of approximately 1.5° and 40 vertical layers (Jungclaus et al.

2013, 2006). This grid setup is a low-resolution (LR) version of the model used for centennial-time-scale simulations in CMIP5. Ocean and atmosphere are coupled daily without flux corrections.

The ocean biogeochemistry module HAMOCC5 (Ilyina et al. 2013; Maier-Reimer et al. 2005) simulates inorganic carbon chemistry and uses an extended NPZD-type description of marine biology in which phytoplankton and zooplankton dynamics depend on temperature, solar radiation, and colimiting nutrients. HAMOCC uses one phytoplankton type for primary production but separates two types of planktonic shell materials (opal and calcium carbonate shells, respectively), which are exported from the euphotic zone with different sinking rates. Additionally, formation and dissolution of sediments is simulated in the model. The land surface model of MPI-ESM, JSBACH (Raddatz et al. 2007), simulates fluxes of energy, water, momentum, and CO_2 between land and atmosphere. Each land grid cell is divided into tiles covered with up to 12 plant functional types. A module for vegetation dynamics (Brovkin et al. 2009) is based on the assumption that competition between different PFTs is determined by their relative competitiveness expressed in annual net primary productivity (NPP), as well as natural and disturbance-driven mortality (fire and wind disturbance).

f. National Centre for Atmospheric Research CESM1-BGC

Version 1 of the Community Earth System Model (CESM1) is the successor to version 4 of the Community Climate System Model (CCSM4), which is a fully coupled, global climate model consisting of land, atmosphere, ocean, and sea ice components (Gent et al. 2011). The experiments examined in this manuscript use a configuration of CESM1 with its biogeochemistry modules enabled, a configuration that is denoted as CESM1-BGC and documented by K. Lindsay et al. (2012, unpublished manuscript). The marine ecosystem module (J. K. Moore et al. 2012, personal communication) utilizes multiple phytoplankton functional groups and a single zooplankton class. Phytoplankton growth is controlled by temperature, light, and available nutrients (N, P, Si, and Fe). The land surface model, CLM4 (Lawrence et al. 2012), includes a biogeochemical module with coupled carbon–nitrogen dynamics, which is denoted in some places as CLM4CN (Thornton et al. 2007, 2009).

The land and ocean components both include aeolian deposition of nitrogen as a forcing of the nitrogen cycle. In the standard 1% increasing CO_2 experiments, this deposition was prescribed with a fixed preindustrial dataset.

g. Norwegian Climate Centre NorESM-ME

The Norwegian Earth System Model (NorESM-ME) is based on the Community Earth System Model (CESM1), which is managed and maintained by the National Center for Atmospheric Research (NCAR), with some modification to the model components. The NorESM-ME adopts the same coupler (CPL7), atmosphere [Community Atmosphere Model, version 4.0 (CAM4)], terrestrial (CLM4), and sea ice [sea ice component version 7 (CICE4)] modules. However, the ocean component is based on the Miami Isopycnic Coordinate Ocean Model (MICOM), which is coupled together with the Hamburg Oceanic Carbon Cycle (HAMOCC) model (Assmann et al. 2010). In addition, the atmospheric chemistry has been modified following Seland et al. (2008).

The HAMOCC ocean carbon cycle model simulates the carbon chemistry based on the Ocean Carbon-Cycle Model Intercomparison Project (OCMIP) protocols. It also implements an NPZD-type ecosystem model with multnutrient limitation for the marine biological production. The gas exchange formulation is based on formulation by Wanninkhof (1992). In addition to biogeochemical processes, the CLM4 model also implements carbon–nitrogen biogeochemistry with prognostic carbon and nitrogen in vegetation, litter, and soil organic matter (Bonan and Levis 2010; Lawrence et al. 2011). Nitrogen deposition for the 1% increasing CO₂ simulations used here was held constant at preindustrial values of 19.45 Tg N yr^{−1}. A more detailed description of the carbon cycle components of NorESM is discussed in Tjiputra et al. (2013).

h. Met Office HadGEM2-ES

HadGEM2-ES (Collins et al. 2011) couples interactive ocean biogeochemistry, terrestrial biogeochemistry and dust, interactive atmospheric chemistry, and aerosol components into an update of the physical model HadGEM1 (Johns et al. 2006). The physical model contains a 40-level 1° × 1°, moving to 1/3° at the equator, ocean and a 38-level 1.875° × 1.25° atmosphere (Martin et al. 2011). HadGEM2-ES has been set up and used to perform CMIP5 simulations as described by Jones et al. (2011).

The ocean biogeochemistry uses the Diat-HadOCC model (I. J. Totterdell and P. R. Halloran 2012, personal communication), an update of HadOCC (Palmer and Totterdell 2001), now simulating diatom and nondiatom phytoplankton functional types; a single zooplankton; and cycling of nitrogen, silica, and iron. Diat-HadOCC is coupled to other Earth system components through the model's physics, iron supplied through dust, air–sea exchange of CO₂, and oceanic emission of dimethylsulfide.

The terrestrial carbon cycle is represented by the Met Office Surface Exchanges Scheme, version 2 (MOSES2) land surface scheme (Essery et al. 2003), which simulates exchange of water, energy, and carbon between the land surface and the atmosphere, and the TRIFFID dynamic global vegetation model (Cox 2001), which simulates the coverage and competition between five plant functional types (broadleaf tree, needleleaf tree, C₃ and C₄ grass, and shrub) and four nonvegetated surface types (bare soil, urban, lakes, and land ice). The soil carbon component has been updated based on the four-pool RothC soil carbon model (Jones et al. 2005).

i. University of Victoria ESCM 2.9

The University of Victoria Earth System Climate Model (UVic ESCM) version 2.9 (Eby et al. 2009) consists of a primitive equation 3D OGCM coupled to a dynamic–thermodynamic sea ice model and an energy–moisture balance model of the atmosphere with dynamical feedbacks (Weaver et al. 2001). The land surface and terrestrial vegetation components are represented by a simplified version of the Hadley Centre's MOSES land surface scheme coupled to the dynamic vegetation model TRIFFID (Meissner et al. 2003). Land carbon fluxes are calculated within MOSES and are allocated to vegetation and soil carbon pools (Matthews et al. 2004). Ocean carbon is simulated by means of an OCMIP-type inorganic carbon–cycle model and an NPZD marine ecosystem model (Schmittner et al. 2007). Sediment processes are represented using an oxic-only model of sediment respiration (Archer 1996).

REFERENCES

- Archer, D., 1996: A data-driven model of the global calcite lysocline. *Global Biogeochem. Cycles*, **10**, 511–526, doi:10.1029/96GB01521.
- Arora, V. K., and G. J. Boer, 2010: Uncertainties in the 20th century carbon budget associated with land use change. *Global Change Biol.*, **16**, 3327–3348.
- , and Coauthors, 2009: The effect of terrestrial photosynthesis down regulation on the twentieth-century carbon budget simulated with the CCCma Earth System Model. *J. Climate*, **22**, 6066–6088.
- , and Coauthors, 2011: Carbon emission limits required to satisfy future representative concentration pathways of greenhouse gases. *Geophys. Res. Lett.*, **38**, L05805, doi:10.1029/2010GL046270.
- Assmann, K. M., M. Bentsen, J. Segschneider, and C. Heinze, 2010: An isopycnic ocean carbon cycle model. *Geosci. Model Dev.*, **3**, 143–167, doi:10.5194/gmd-3-143-2010.
- Aumont, O., and L. Bopp, 2006: Globalizing results from ocean in situ iron fertilization studies. *Global Biogeochem. Cycles*, **20**, GB2017, doi:10.1029/2005GB002591.
- Bacastow, R., and E. Maier-Reimer, 1990: Ocean-circulation model of the carbon cycle. *Climate Dyn.*, **4**, 95–125.

- Boer, G. J., and V. Arora, 2009: Temperature and concentration feedbacks in the carbon cycle. *Geophys. Res. Lett.*, **36**, L02704, doi:10.1029/2008GL036220.
- , and —, 2010: Geographic aspects of temperature and concentration feedbacks in the carbon budget. *J. Climate*, **23**, 775–784.
- , and —, 2013: Feedbacks in emissions-driven and concentration-driven global carbon budgets. *J. Climate*, **26**, 3326–3341.
- Bonan, G. B., and S. Levis, 2010: Quantifying carbon-nitrogen feedbacks in the Community Land Model (CLM4). *Geophys. Res. Lett.*, **37**, L07401, doi:10.1029/2010GL042430.
- Boucher, O., A. Jones, and R. Betts, 2009: Climate response to the physiological impact of carbon dioxide on plants in the Met Office Unified Model HadCM3. *Climate Dyn.*, **32**, 237–249.
- Broecker, W. S., and T.-H. Peng, 1986: Carbon cycle: 1985—Glacial to interglacial changes in the operation of the global carbon cycle. *Radiocarbon*, **28**, 309–327.
- Brovkin, V., T. Raddatz, C. H. Reick, M. Claussen, and V. Gayler, 2009: Global biogeophysical interactions between forest and climate. *Geophys. Res. Lett.*, **36**, L07405, doi:10.1029/2009GL037543.
- Christian, J. R., and Coauthors, 2010: The global carbon cycle in the Canadian Earth System Model (CanESM1): Preindustrial control simulation. *J. Geophys. Res.*, **115**, G03014, doi:10.1029/2008JG000920.
- Coleman, K., and D. S. Jenkinson, 1999: ROTHC-26.3: A model for the turnover of carbon in soil. IACR Rep., 43 pp [Available online at http://www.rothamsted.ac.uk/aen/carbon/mod26_3_dos.pdf].
- Collins, W. J., and Coauthors, 2011: Development and evaluation of an Earth-system model—HadGEM2. *Geosci. Model Dev.*, **4**, 1051–1075.
- Cox, P. M., 2001: Description of the TRIFFID dynamic global vegetation model. Met Office Hadley Centre Tech. Note 24, 17 pp.
- Dufresne, J.-L., and Coauthors, 2013: Climate change projections using the IPSL-CM5 Earth System Model: From CMIP3 to CMIP5. *Climate Dyn.*, **40**, 2123–2165, doi:10.1007/s00382-012-1636-1.
- Eby, M., and Coauthors, 2009: Lifetime of anthropogenic climate change: Millennial time scales of potential CO₂ and surface temperature perturbations. *J. Climate*, **22**, 2501–2511.
- Essery, R. L. H., M. J. Best, R. A. Betts, P. M. Cox, and C. M. Taylor, 2003: Explicit representation of subgrid heterogeneity in a GCM land-surface scheme. *J. Hydrometeorol.*, **4**, 530–543.
- Fichefet, T., and M. A. Morales Maqueda, 1997: Sensitivity of a global sea ice model to the treatment of ice thermodynamics and dynamics. *J. Geophys. Res.*, **102** (C6), 12 609–12 646.
- Friedlingstein, P., J.-L. Dufresne, P. M. Cox, and P. Rayner, 2003: How positive is the feedback between climate change and the carbon cycle? *Tellus*, **55B**, 692–700.
- , and Coauthors, 2006: Climate–carbon cycle feedback analysis: Results from the C⁴MIP model intercomparison. *J. Climate*, **19**, 3337–3353.
- Gent, P. R., and Coauthors, 2011: The Community Climate System Model version 4. *J. Climate*, **24**, 4973–4991.
- Goodwin, P., and T. M. Lenton, 2009: Quantifying the feedback between ocean heating and CO₂ solubility as an equivalent carbon emission. *Geophys. Res. Lett.*, **36**, L15609, doi:10.1029/2009GL039247.
- Gregory, J. M., C. D. Jones, P. Cadule, and P. Friedlingstein, 2009: Quantifying carbon cycle feedbacks. *J. Climate*, **22**, 5232–5250.
- Griffies, S. M., and Coauthors, 2005: Formulation of an ocean model for global climate simulations. *Ocean Sci.*, **1**, 45–79.
- Hasumi, H., 2007: CCSR Ocean Component Model (COCO) version 4.0. The University of Tokyo Center for Climate System Research Rep., 111 pp. [Available online at <http://ccsr.aori.u-tokyo.ac.jp/~hasumi/COCO/coco4.pdf>].
- Heinze, C., A. Hupe, E. Maier-Reimer, N. Dittert, and O. Ragueneau, 2003: Sensitivity of the marine biospheric Si cycle for biogeochemical parameter variations. *Global Biogeochem. Cycles*, **17**, 1086, doi:10.1029/2002GB001943.
- Hourdin, F., and Coauthors, 2006: The LMDZ4 general circulation model: Climate performance and sensitivity to parametrized physics with emphasis on tropical convection. *Climate Dyn.*, **27**, 787–813, doi:10.1007/s00382-006-0158-0.
- Ilyina, T., K. D. Six, J. Segschneider, E. Maier-Reimer, H. Li, and I. Núñez-Riboni, 2013: The global ocean biogeochemistry model HAMOCC: Model architecture and performance as component of the MPI-Earth System Model in different CMIP5 experimental realizations. *J. Adv. Model. Earth Syst.*, doi:10.1002/jame.20017, in press.
- Ito, A., and T. Oikawa, 2002: A simulation model of the carbon cycle in land ecosystems (Sim-CYCLE): A description based on dry-matter production theory and plot-scale validation. *Ecol. Modell.*, **151** (2–3), 143–176.
- Ji, J., M. Huang, and K. Li, 2008: Prediction of carbon exchange between China terrestrial ecosystem and atmosphere in 21st century. *Sci. China*, **51D**, 885–898.
- Johns, T. C., and Coauthors, 2006: The new Hadley Centre climate model (HadGEM1): Evaluation of coupled simulations. *J. Climate*, **19**, 1327–1353.
- Jones, C., C. McConnell, K. Coleman, P. Cox, P. Falloon, D. Jenkinson, and D. Powlson, 2005: Global climate change and soil carbon stocks; predictions from two contrasting models for the turnover of organic carbon in soil. *Global Change Biol.*, **11**, 154–166.
- , and Coauthors, 2011: The HadGEM2-ES implementation of CMIP5 centennial simulations. *Geosci. Model Dev.*, **4**, 543–570, doi:10.5194/gmd-4-543-2011.
- Jungclaus, J. H., and Coauthors, 2006: Ocean circulation and tropical variability in the coupled model ECHAM5/MPI-OM. *J. Climate*, **19**, 3952–3972.
- , and Coauthors, 2013: Characteristics of the ocean simulations in MPIOM, the ocean component of the MPI-Earth System Model. *J. Adv. Model. Earth Syst.*, doi:10.1002/jame.20023, in press.
- Kawamiya, M., M. J. Kishi, and N. Sugihara, 2000: An ecosystem model for the North Pacific embedded in a general circulation model. Part II: Mechanisms forming seasonal variations of chlorophyll. *J. Mar. Syst.*, **25**, 159–178.
- Krinner, G., and Coauthors, 2005: A dynamic global vegetation model for studies of the coupled atmosphere-biosphere system. *Global Biogeochem. Cycles*, **19**, GB1015, doi:10.1029/2003GB002199.
- Lawrence, D. M., and Coauthors, 2011: Parameterization improvements and functional and structural advances in version 4 of the Community Land Model. *J. Adv. Model. Earth Syst.*, **3**, doi:10.1029/2011MS000045.
- , K. W. Oleson, M. G. Flanner, C. G. Fletcher, P. J. Lawrence, S. Levis, S. C. Swenson, and G. B. Bonan, 2012: The CCSM4 land simulation, 1850–2005: Assessment of surface climate and new capabilities. *J. Climate*, **25**, 2240–2260.
- Luo, Y., D. A. Sims, R. B. Thomas, D. T. Tissue, and J. T. Ball, 1996: Sensitivity of leaf photosynthesis to CO₂ concentration

- is an invariant function for C3 plants: A test with experimental data and global applications. *Global Biogeochem. Cycles*, **10**, 209–222.
- MacDougall, A. H., C. A. Avis, and A. J. Weaver, 2012: Significant contribution to climate warming from the permafrost carbon feedback. *Nat. Geosci.*, **5**, 719–721, doi:10.1038/ngeo1573.
- Madec, G., 2008: NEMO ocean engine. IPSL Tech. Note, 332 pp.
- Maier-Reimer, E., I. Kriest, J. Segsneider, and P. Wetzel, 2005: The Hamburg Ocean Carbon Cycle Model HAMOCC5.1—Technical description release 1.1. MPI Earth System Science Rep. 14, 57 pp.
- Marti, O., and Coauthors, 2010: Key features of the IPSL ocean atmosphere model and its sensitivity to atmospheric resolution. *Climate Dyn.*, **34**, 1–26, doi:10.1007/s00382-009-0640-6.
- Martin, G. M., and Coauthors, 2011: The HadGEM2 family of Met Office Unified Model Climate configurations. *Geosci. Model Dev.*, **4**, 723–757.
- Matthews, H. D., A. J. Weaver, K. J. Meissner, N. P. Gillett, and M. Eby, 2004: Natural and anthropogenic climate change: Incorporating historical land cover change, vegetation dynamics and the global carbon cycle. *Climate Dyn.*, **22**, 461–479, doi:10.1007/s00382-004-0392-2.
- Meissner, K. J., A. J. Weaver, H. D. Matthews, and P. M. Cox, 2003: The role of land surface dynamics in glacial inception: A study with the UVic Earth System Model. *Climate Dyn.*, **21**, 515–537, doi:10.1007/s00382-003-0352-2.
- Murray, R. J., 1996: Explicit generation of orthogonal grids for ocean models. *J. Comput. Phys.*, **126**, 251–273.
- Nozawa, T., T. Nagashima, T. Ogura, T. Yokohata, N. Okada, and H. Shiogama, 2007: *Climate Change Simulations with a Coupled Ocean-Atmosphere GCM Called the Model for Interdisciplinary Research on Climate: MIROC. Supercomputer Monogr. Rep.*, Vol. 12, Center for Global Environmental Research, 79 pp.
- Oschlies, A., 2001: Model-derived estimates of new production: New results point towards lower values. *Deep-Sea Res. II*, **48**, 2173–2197.
- Palmer, J. R., and I. J. Totterdell, 2001: Production and export in a global ocean ecosystem model. *Deep-Sea Res. I*, **48**, 1169–1198, doi:10.1016/S0967-0637(00)00080-7.
- Plattner, G.-K., and Coauthors, 2008: Long-term climate commitments projected with climate–carbon cycle models. *J. Climate*, **21**, 2721–2751.
- Qian, H., R. Joseph, and N. Zeng, 2010: Enhanced terrestrial carbon uptake in the northern high latitudes in the 21st century from the Coupled Carbon Cycle Climate Model Intercomparison Project model projections. *Global Change Biol.*, **16**, 641–656.
- Raddatz, T. J., and Coauthors, 2007: Will the tropical land biosphere dominate the climate–carbon cycle feedback during the twenty-first century? *Climate Dyn.*, **29**, 565–574, doi:10.1007/s00382-007-0247-8.
- Roeckner, E., and Coauthors, 2003: The atmospheric general circulation model ECHAM5. Part I: Model description. Max Planck Institute for Meteorology Rep. 349, 127 pp.
- Roy, T., and Coauthors, 2011: Regional impacts of climate change and atmospheric CO₂ on future ocean carbon uptake: A multimodel linear feedback analysis. *J. Climate*, **24**, 2300–2318.
- Sato, H., A. Itoh, and T. Kohyama, 2007: SEIB-DGVM: A new Dynamic Global Vegetation Model using a spatially explicit individual-based approach. *Ecol. Modell.*, **200**, 279–307, doi:10.1016/j.ecolmodel.2006.09.006.
- Schmittner, A., A. Oschlies, H. D. Matthews, and E. D. Galbraith, 2007: Future changes in climate, ocean circulation, ecosystems and biogeochemical cycling simulated for a business-as-usual CO₂ emission scenario until year 4000 AD. *Global Biogeochem. Cycles*, **22**, 1013–1034, doi:10.1029/2007GB002953.
- Seland, Ø., T. Iversen, A. Kirkevåg, and T. Storelvmo, 2008: Aerosol-climate interactions in the CAM-Oslo atmospheric GCM and investigation of associated basic shortcomings. *Tellus*, **60A**, 459–491.
- Stevens, B., and Coauthors, 2013: The atmospheric component of the MPI-M Earth System Model: ECHAM6. *J. Adv. Model. Earth Syst.*, doi:10.1002/jame.20015, in press.
- Sudo, K., M. Takahashi, J. Kurokawa, and H. Akimoto, 2002: CHASER: A global chemical model of the troposphere 1. Model description. *J. Geophys. Res.*, **107**, 4339, doi:10.1029/2001JD001113.
- Takata, K., S. Emori, and T. Watanabe, 2003: Development of the minimal advanced treatments of surface interaction and runoff. *Global Planet. Change*, **38**, 209–222, doi:10.1016/S0921-8181(03)00030-4.
- Takemura, T., H. Okamoto, Y. Maruyama, A. Numaguti, A. Higurashi, and T. Nakajima, 2000: Global three-dimensional simulation of aerosol optical thickness distribution of various origins. *J. Geophys. Res.*, **105** (D14), 17 853–17 873.
- Taylor, K. E., R. J. Stouffer, and G. A. Meehl, 2012: An overview of CMIP5 and the experiment design. *Bull. Amer. Meteor. Soc.*, **93**, 485–498.
- Thornton, P. E., J.-F. Lamarque, N. A. Rosenbloom, and N. M. Mahowald, 2007: Influence of carbon-nitrogen cycle coupling on land model response to CO₂ fertilization and climate variability. *Global Biogeochem. Cycles*, **21**, GB4018, doi:10.1029/2006GB002868.
- , and Coauthors, 2009: Carbon-nitrogen interactions regulate climate-carbon cycle feedbacks: Results from an atmosphere-ocean general circulation model. *Biogeosciences*, **6**, 2099–2120, doi:10.5194/bg-6-2099-2009.
- Tjiputra, J. F., C. Roelandt, M. Bentsen, D. M. Lawrence, T. Lorentzen, J. Schwinger, Ø. Seland, and C. Heinze, 2013: Evaluation of the carbon cycle components in the Norwegian Earth System Model (NorESM). *Geosci. Model Dev.*, **6**, 301–325, doi:10.5194/gmd-6-301-2013.
- Wanninkhof, R., 1992: Relationship between wind speed and gas exchange over the ocean. *J. Geophys. Res.*, **97** (C5), 7373–7382.
- Watanabe, S., H. Miura, M. Sekiguchi, T. Nagashima, K. Sudo, S. Emori, and M. Kawamiya, 2008: Development of an atmospheric general circulation model for integrated Earth system modeling on the Earth Simulator. *J. Earth Simul.*, **9**, 27–35.
- , and Coauthors, 2011: MIROC-ESM 2010: Model description and basic results of CMIP5-20c3m experiments. *Geosci. Model Dev.*, **4**, 845–872.
- Weaver, A. J., and Coauthors, 2001: The UVic earth system climate model: Model description, climatology, and applications to past, present and future climates. *Atmos.–Ocean*, **39**, 361–428, doi:10.1080/07055900.2001.9649686.
- Weiss, R. F., 1974: Carbon dioxide in water and seawater: The solubility of a non-ideal gas. *Mar. Chem.*, **2**, 203–215.
- Wu, T., 2012: A mass-flux cumulus parameterization scheme for large-scale models: Description and test with observations. *Climate Dyn.*, **38**, 725–744, doi:10.1007/s00382-011-0995-3.

- , R. Yu, and F. Zhang, 2008: A modified dynamic framework for atmospheric spectral model and its application. *J. Atmos. Sci.*, **65**, 2235–2253.
- , and Coauthors, 2010: The Beijing Climate Center atmospheric general circulation model: Description and its performance for the present-day climate. *Climate Dyn.*, **34**, 123–147.
- , and Coauthors, 2013: Global carbon budgets simulated by the Beijing Climate Center Climate System Model for the last century. *J. Geophys. Res.*, **118**, 4326–4347, doi:10.1002/jgrd.50320.
- Yamanaka, Y., and E. Tajika, 1996: The role of the vertical fluxes of particulate organic matter and calcite in the oceanic carbon cycle: Studies using an ocean biogeochemical general circulation model. *Global Biogeochem. Cycles*, **10**, 361–382.
- Zaehle, S., P. Friedlingstein, and A. D. Friend, 2010: Terrestrial nitrogen feedbacks may accelerate future climate change. *Geophys. Res. Lett.*, **37**, L01401, doi:10.1029/2009GL041345.
- Zahariev, K., J. R. Christian, and K. L. Denman, 2008: Preindustrial, historical, and fertilization simulations using a global ocean carbon model with new parameterizations of iron limitation, calcification, and N₂ fixation. *Prog. Oceanogr.*, **77**, 56–82.
- Zhang, Q., Y. P. Wang, A. J. Pitman, and Y. J. Dai, 2011: Limitations of nitrogen and phosphorous on the terrestrial carbon uptake in the 20th century. *Geophys. Res. Lett.*, **38**, L22701, doi:10.1029/2011GL049244.
- Zickfeld, K., M. Eby, H. D. Matthews, A. Schmittner, and A. J. Weaver, 2011: Nonlinearity of carbon cycle feedbacks. *J. Climate*, **24**, 4254–4274.